ACTIVITY OF CARBON SUPPORTED PLATINUM NANOPARTICLES TOWARD METHANOL OXIDATION REACTIONS: ROLE OF METAL PRECURSOR AND NEW SURFACTANTS

A THESIS SUBMITTED TO
THE GRADUATE SCHOOL OF NATURAL AND APPLIED SCIENCES
OF
THE MIDDLE EAST TECHNICAL UNIVERSITY

BY

SELDA ŞEN

IN PARTIAL FULFILLMENT OF THE REQUIREMENTS
FOR
THE DEGREE OF MASTER OF SCIENCE
IN
CHEMISTRY

JANUARY 2008

Approval of the thesis:

ACTIVITY OF CARBON SUPPORTED PLATINUM NANOPARTICLES TOWARD METHANOL OXIDATION REACTIONS: ROLE OF METAL PRECURSOR AND NEW SURFACTANTS

submitted by **SELDA ŞEN** in partial fulfillment of the requirements for the degree of **Master of Science in Chemistry Department, Middle East Technical University** by,

Prof. Dr. Canan Özgen _____
Dean, Graduate School of **Natural and Applied Sciences**

Prof. Dr. Ahmet Önal _____
Head of Department, **Chemistry**

Assoc. Prof. Dr. Gülsün Gökağaç _____
Supervisor, **Chemistry Dept., METU**

Examining Committee Members :

Prof. Dr. Hüseyin İşçi _____
Chemistry Dept., METU

Assoc. Prof. Dr. Gülsün Gökağaç _____
Chemistry Dept., METU

Prof. Dr. İnci Eroğlu _____
Chemical Engineering Dept., METU

Prof. Dr. Ceyhan Kayran _____
Chemistry Dept., METU

Asst. Prof. Dr. Ayşen Yılmaz _____
Chemistry Dept., METU

Date: 25/01/2008

I hereby declare that all information in this document has been obtained and presented in accordance with academic rules and ethical conduct. I also declare that, as required by these rules and conduct, I have fully cited and referenced all material and results that are not original to this work.

Name, Last name : Selda ŞEN

Signature :

ABSTRACT

ACTIVITY OF CARBON SUPPORTED PLATINUM NANOPARTICLES CATALYSTS TOWARD METHANOL OXIDATION REACTION: ROLE OF METAL PRECURSOR AND A NEW SURFACTANT

Şen, Selda
M.S., Department of Chemistry
Supervisor: Assoc. Prof. Dr. Gülsün Gökağaç

January 2008, 55 pages

In this thesis, carbon supported platinum nanoparticle catalysts were prepared using $PtCl_4$ and H_2PtCl_6 as starting materials and 1-heptanethiol, tert-nonyl mercaptan, 1-hexadecanethiol, 1-octadecanethiol as surfactants. These new catalysts were employed for methanol oxidation reaction which are used for direct methanol fuel cells. Tert-nonyl mercaptane was used for the first time in this type of reaction and the other surfactants were used for comparison of the catalysts performance. Cyclic voltammetry (CV), X-ray photoelectron spectroscopy (XPS), X-ray diffraction (XRD) and transmission electron microscopy (TEM) were used in order to determine the nature of the catalysts.

The average platinum crystallite particle sizes of all prepared catalysts were determined by both X-ray diffraction and transmission electron microscopy. It was found that platinum crystallizes in face-centered cubic structure and the surfactant play an important role on the size of platinum nanoparticles, branch surfactant, such as tert-nonyl mercaptane, causes an increase in the size of platinum nanoparticles, about 3 nm, compared to linear surfactant, such as 1-heptanethiol, about 2 nm.

The oxidation states of platinum and their ratios were determined by XPS technique. These results indicated that platinum has two different oxidation states, zero and +4, and Pt(0) to Pt(IV) ratio is about 7.5 to 2.5. In addition to this, O 1s region of XPS was also examined and found that the surface of all of the catalysts covered by adsorbed hydroxide except the catalyst which was prepared by $PtCl_4$ and tert-nonyl mercaptane (Catalyst IIa), where adsorption of water were observed and the catalyst which was prepared by H_2PtCl_6 and tert-nonyl mercaptane (Catalysts IIb), where adsorption of 65% of hydroxide and 35% of water were identified.

Electrochemical studies indicated that Catalyst IIa has the maximum activity (~342 A/gPt at 0.612 V) towards methanol oxidation reaction while Catalyst IIIb (H_2PtCl_6 and 1-hexanethiol were used to prepare this catalyst) has the minimum activity (~91A/gPt at 0.580V). XRD, TEM and XPS results indicated that the optimum catalyst for methanol oxidation reaction contains about 3 nm of platinum nanoparticles, adsorbed hydroxide and water on the surface of catalyst, but sulphur. These results are in agreement with the proposed mechanism.

Keywords: Direct Methanol Fuel Cells, Platinum Nanoparticles, Carbon-Supported Thiol Stabilized Catalysts, Cyclic Voltammetry, Transmission Electron Microscopy, X-ray Photoelectron Spectroscopy.

ÖZ

KARBON DESTEKLİ PLATİN NANOPARÇACIKLI KATALİZÖRLERİN METANOL YÜKSELTGENME TEPKİMESİNE KARŞI AKTİVİTELERİ: BAŞLANGIÇ METAL BİLEŞİKLERİNİN VE YENİ SÜRFAKTANTIN ROLLERİ

Şen, Selda
Yüksek Lisans, Kimya Bölümü
Tez Yöneticisi: Doç. Dr. Gülsün Gökağaç

Ocak 2008, 55 sayfa

Bu çalışmada, başlangıç maddesi olarak $PtCl_4$ ve H_2PtCl_6 bileşikleri, sürfaktant olarak da 1-heptantiol, tert-nonil merkaptan, 1-hekzadekantiol ve 1-oktadekantiol kullanılarak, karbon destekli platin nanoparçacıklı katalizörler hazırlanmıştır. Bu yeni katalizörler doğrudan metanol yakıt hücrelerinde kullanılan metanol yükseltgenme tepkimesi için kullanılmıştır. Bu tip tepkimede tert-nonil merkaptan ilk kez kullanılmıştır. Diğer sürfaktantlar ise katalizörlerin performanslarını karşılaştırmak amacıyla kullanılmıştır. Hazırlanan katalizörlerin doğasının aydınlatılmasında dönüşümlü voltametre (CV), X-ışınları fotoelektron spektroskopisi (XPS), X-ışınları kırınımı (XRD) ve transmisyon (geçirmeli) elektron mikroskopu (TEM) tekniklerinden faydalanılmıştır.

Hazırlanan katalizörlerdeki ortalama platin parçacıklarının büyüklüğü X-ışınları kırınımı (XRD) ve transmisyon elektron mikroskobu (TEM) yardımıyla belirlenmiştir. Bu çalışmalar platin kristallerinin yüzey merkezli kübik bir yapıya sahip olduklarını ve katalizör hazırlamada kullanılan sürfaktantların yapısının platin nanoparçacıklarının büyüklüğünün tayininde önemli rol oynadığını göstermiştir. Örneğin, tert-nonil merkaptan gibi dallanmış yapıya sahip bir sürfaktantla hazırlanmış platin nanoparçacıklı katalizörler (yaklaşık 3 nm), lineer yapıya (1-

heptantiol gibi) sahip olan sürfaktantlarla hazırlanmış katalizörlere (yaklaşık 2 nm) kıyasla daha büyüktür.

X-ışınları fotoelektron spektroskopisi (XPS) yardımıyla hazırlanan katalizörlerdeki platinin oksidasyon değerlikleri ve bunların birbirlerine oranları belirlenmiştir. Buna göre, hazırlanan katalizörlerdeki platinin '0' ve '+4' değerliklerine sahip olduğu ve Pt(0)/Pt(IV) oranının yaklaşık 7.5 / 2.5 olduğu bulunmuştur. Buna ek olarak, aynı teknikle O 1s bölgesi incelenmiş ve $PtCl_4$ ile tert-nonyl merkaptan (Katalizör IIa) kullanılarak hazırlanan katalizörde su molekülünün katalizör yüzeyine bağlandığı ve H_2PtCl_6 ile tert-nonyl merkaptan (Katalizör IIb) kullanılarak hazırlanan katalizörde ise hem suyun hem de hidroksit iyonlarının (65 % hidroksit ve 35 % su) yüzeyde tutulduğu gözlenirken, diğer tüm katalizörlerde ise hidroksit iyonlarının katalizör yüzeyinde tutulduğu gözlemlenmiştir.

Hazırlanan katalizörler üzerinde yapılan elektrokimyasal çalışmalarda H_2PtCl_6 ve 1-hekzadekantiol ile hazırlanan katalizör (Katalizör IIIb) metanol yükseltgenme tepkimesine karşı en düşük aktiviteyi (~91 A/g Pt at 0.580V) gösterirken, Katalizör IIa'nın en yüksek aktiviteye sahip olduğu bulunmuştur (~342 A/g Pt at 0.612 V). XRD, TEM ve XPS sonuçlarına göre metanol yükseltgenme tepkimesi için en uygun katalizörün yaklaşık 3 nm büyüklüğündeki platin nanoparçacıkları içeren, yüzeyinde hidroksit ve su adsorbe eden ve sülfür içermeyen katalizörler olduğu bulunmuştur. Bu sonuçlar da önerilen mekanizma ile uyum içerisindedir.

Anahtar Kelimeler: Doğrudan Metanol Yakıt Pilleri, Platin Nanoparçacıkları, Karbon Destekli ve Tiol ile Stabilize Edilmiş Katalizörler, Dönüşümlü Voltametre, Transmisyon (Geçirmeli) Elektron Mikroskopisi

To My Husband

ACKNOWLEDGEMENTS

First, the author wishes to express her deepest gratitude to her supervisor, Assoc. Prof. Dr. Gülsün Gökağaç, for her guidance, advice, criticism, encouragements, continuous interest, help, support, patience and insight throughout the research.

The author thanks specially goes to Fatih ŞEN for his great support, trust, patience, suggestions, comments and love. This work couldn't be accomplished without him.

The author is grateful to her parents for their endless love, support, trust and encouragement.

The author would like to thank TUBITAK for financial support, Asst. Prof. Dr. Ayşen YILMAZ for XRD measurements and her interpretation related with these measurements and also METU Chemistry Department for their sincere support during her M.S. study.

Lastly, the author would like to thank the staff of central laboratory of METU (particularly Selda Keskin).

TABLE OF CONTENTS

LIST OF TABLES

TABLES

LIST OF FIGURES

FIGURES

CHAPTER 1

INTRODUCTION

1.1. FUEL CELLS, THEIR ADVANTAGES AND DISADVANTAGES

A fuel cell is an electrochemical energy conversion device. It produces electricity from external supplies of fuel (on the anode side) and oxidant (on the cathode side). These react in the presence of an electrolyte. Generally, the reactants flow in and reaction products flow out while the electrolyte remains in the cell. Fuel cells can operate virtually continuously as long as the necessary flows are maintained.

Fuel cells differ from batteries in that they consume reactant, which must be replenished, while batteries store electrical energy chemically in a closed system. Additionally, while the electrodes within a battery react and change as a battery is charged or discharged, a fuel cell's electrodes are catalytic and relatively stable (Bockris, 1969).

Many combinations of fuel and oxidant are possible. A hydrogen cell uses hydrogen as fuel and oxygen as oxidant. Other fuels include hydrocarbons and alcohols. Other oxidants include air, chlorine and chlorine dioxide . The principle of the fuel cell was discovered by German scientist Christian Friedrich Schönbein in 1838 and published in the January 1839 edition of the "Philosophical Magazine"(Groove, 1839). Based on this work, the first fuel cell was developed by Welsh scientist Sir William Robert Grove in 1843. The fuel cell that he made used similar materials to today's phosphoric-acid fuel cell. The principle that he discovered remains unchanged today: "*A fuel cell is an electrochemical 'device' that continuously converts chemical energy into electrical energy (and some heat) for as long as fuel and oxidant are supplied* ".

Obviously, fuel cells have various advantages compared to conventional power sources, such as internal combustion engines or batteries. Although some of the fuel cells' attributes are only valid for some applications, most advantages are more general. However, there are some disadvantages facing developers and the commercialisation of fuel cells as well.

Advantages

- Fuel cells eliminate pollutants such as SO_2, NO_x, CO and soot caused by burning fossil fuels.
- If the hydrogen used as a fuel, then the fuel cells eliminates greenhouse gases.
- Fuel cells do not need conventional fuels such as oil or gas and can therefore eliminate economic dependence on other countries.
- Installation of smaller stationary fuel cells leads to a more stabilised and decentralised power grid.
- Fuel cells have a higher efficiency than diesel or gas engines.
- Most fuel cells operate silently, compared to internal combustion engines.
- Low temperature fuel cells (PEM, DMFC) have low heat transmission which makes them ideal for military applications.
- Operating times are much longer than with batteries, since doubling the operating time needs only doubling the amount of fuel and not the doubling of the capacity of the unit itself.
- Fuel cells have no "memory effect" when they are getting refuelled.
- The maintenance of fuel cells is simple since there are few moving parts in the system.

Disadvantages

- Fuelling of some of fuel cells is still a major problem for example the production, transportation, distribution and storage of hydrogen is difficult for hydrogen-air fuel cells.
- Reforming hydrocarbons via reformer to produce hydrogen is technically challenging and not clearly environmentally friendly.

- The refuelling and the starting time of fuel cell vehicles are longer and the driving range is shorter than in a “normal” car.
- Fuel cells are in general slightly bigger than comparable batteries or engines. However, the size of the units is decreasing.
- Fuel cells are currently very expensive to produce, since most units are hand-made.
- Some fuel cells use expensive catalytic materials such as platinum and ruthenium.
- The technology is not yet fully developed and few products are available (Gökağaç, 1993a).

1.2. THE HISTORY OF FUEL CELLS

In 1800, British scientists William Nicholson and Anthony Carlisle had described the process of using electricity to decompose water into hydrogen and oxygen. William Robert Grove, however took this idea one step further or, more accurately, one step in reverse in 1838 (Figure 1.1.).

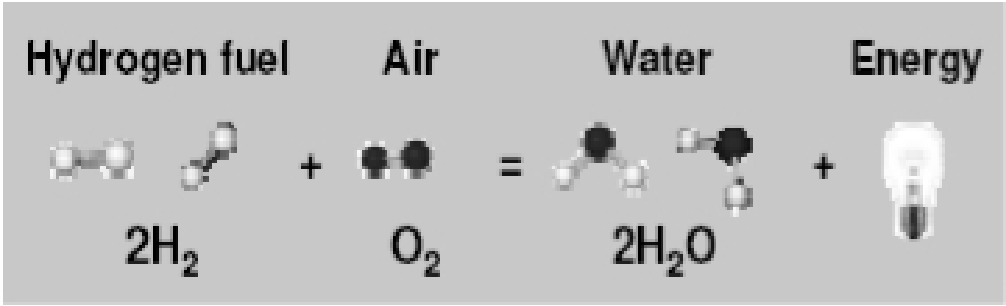

Figure 1.1. Chemical reaction behind fuel cells.

Grove discovered that by arranging two platinum electrodes with one end of each immersed in a container of sulfuric acid and the other ends separately sealed in containers of oxygen and hydrogen, a constant current would flow between the electrodes. The sealed containers held water as well as the gases, and he noted that

the water level rose in both tubes as the current flowed. By combining several sets of these electrodes in a series curcuit, he created what he called a "gas battery"- the first fuel cell, Figure 1.2 (Grove, 1839).

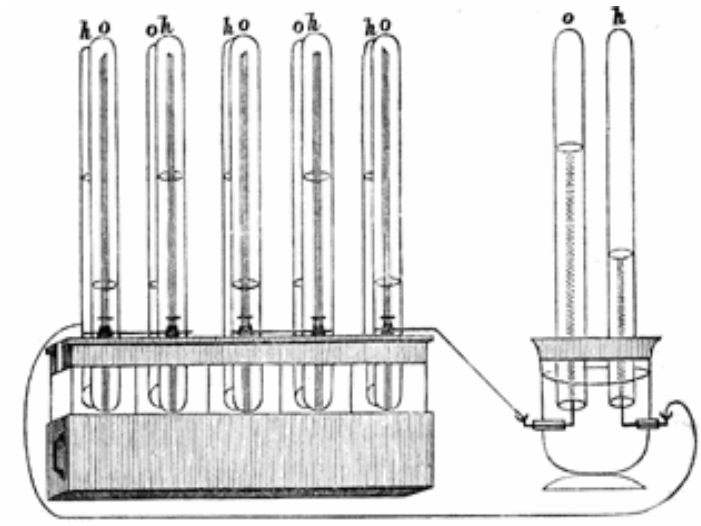

Figure 1.2. Grove's Fuel Cell Diagram Courtesy of the Smithsonian National Museum of Natural History.

In 1889, Ludwig Mond and assistant Carl Langer described their experiments with a hydrogen-oxygen fuel cell that attained 6 amps per square foot (measuring the surface area of the electrode) at 0.73 volts. Mond and Langer's cell used electrodes of thin, perforated platinum (Mond, 1889).

Friedrich Wilhelm Ostwald, a founder of the field of physical chemistry, provided much of the theoretical understanding of how fuel cells operate. In 1893, he experimentally determined the interconnected roles of the various components of the fuel cell: electrodes, electrolyte, oxidizing and reducing agents, anions, and cations. Grove had speculated that the action in his gas battery occurred at the point of contact between electrode, gas, and electrolyte, but was at a loss to explain further.

Ostwald, drawing on his pioneering work in relating physical properties and chemical reactions, solved the puzzle of Grove's gas battery. His exploration of the underlying chemistry of fuel cells laid the groundwork for later fuel cell researchers (Ostwalt, 1894).

Haber (Haber, 1905), Nernst (Nernst, 1912) and Bauer (Bauer, 1912) built a practical cell with solid electrolytes in the beginning of 1900. In 1913, Siegl (Siegl, 1913) reduced the cost of the electrodes by putting platinum on a carbon support. In 1928, Muller et al. (Muller, 1923 and 1928) then investigated the oxidation of liquid organic fuels on different fuel metals, in aqueous solutions. However, none of these attempts led to an economically satisfactory fuel cell. Therefore, in the following years interest in fuel cells waned.

Francis Thomas Bacon (1904 -1992) began researching alkali electrolyte fuel cells in the late 1930s. In 1939, he built a cell that used nickel gauze electrodes and operated under pressure as high as 3000 psi. During World War II, Bacon worked on developing a fuel cell that could be used in Royal Navy submarines, and in 1958 demonstrated an alkali cell using a stack of 10-inch diameter electrodes for Britain's National Research Development Corporation. Though expensive, Bacon's fuel cells proved reliable enough to attract the attention of Pratt & Whitney. The company licensed Bacon's work for the Apollo spacecraft fuel cells (Bacon, 1960).

The recent history of the fuel cell can be thought of as beginning in the early 1960s. A new US government agency, the National Aeronautics and Space Administration (NASA), was looking for a way to power a series of upcoming manned space flights. NASA had already ruled out using batteries as they were too heavy, solar energy as it was too expensive and nuclear power as it was too risky and began to look around for an alternative. The fuel cell was lighted upon as a possible solution and NASA awarded a number of research contracts to develop a practical working design.

This search led to the development of the first Proton Exchange Membrane (PEM). In 1955 Willard Thomas Grubb, a chemist working for General Electric (GE), further

modified the original fuel cell design by using a sulphonated polystyrene ion-exchange membrane as the electrolyte. Three years later another GE chemist, Leonard Niedrach, devised a way of depositing platinum on to this membrane and this became known as the 'Grubb-Niedrach fuel cell' (Grubb, 1960). GE went on to develop this technology with NASA, leading to it being used on the Gemini space project. This was the first commercial use of a fuel cell.

In the early 1960s the aircraft manufacturer Pratt & Whitney licensed the Bacon patents for the alkaline fuel cell. The company modified the original design in order to reduce the weight and developed a cell that proved to be longer-lasting than the GE PEM design. As a result Pratt and Whitney won a contract from NASA to supply these fuel cells to the Apollo spacecraft and alkali cells have since been used on most subsequent missions, including the Space Shuttle flights. An additional benefit of using fuel cell power is that they produce drinkable water as a by-product. Despite this flurry of interest in space applications, there was little development work at this time on fuel cells for more down to earth applications (Linden, 1984).

An oil embargo in 1973 kick-started renewed interest in fuel cell power for terrestrial applications as governments looked to reduce their dependence on petroleum imports. A number of companies and government organisations began to undertake serious research into overcoming the obstacles to widespread commercialisation of the fuel cell. Throughout the 1970s and 1980s a huge research effort was dedicated to developing the materials needed, identifying the optimum fuel source and drastically reducing the cost of this exotic technology (Cohn, 1965).

Finally, in the 1990s, over 150 years after Grove's experiments, the promise of inexpensive, clean, renewable energy began to look as if it might become reality as the first viable fuel cells were unveiled. Technical breakthroughs during the decade included the launch of the first fuel cell-powered vehicle in 1993 by the Canadian company Ballard. Two years later a fuel cell stack with a power density of 1 kW per litre was demonstrated by Ballard and Daimler Benz.

In the last few years we have seen fuel cells installed in hospitals and schools and many of the major automotive companies have unveiled prototype fuel cell powered

cars. Trials of fuel cell powered busses have taken place in Chicago and Vancouver with other cities in North America and Europe looking to take delivery of these vehicles in the near future. A more exhaustive list of the work undertaken by the major players in this field in recent years has been compiled under the section on company information.

Over the coming decades concerns over depleting stocks of natural resources and a growing awareness of the environmental damage caused by widespread burning of fossil fuels will help to drive the development of fuel cells for both transport and stationary power sources. A nineteenth century scientific curiosity may well transpire to be the power source for the twenty-first century and beyond.

1.3. APPLICATIONS OF FUEL CELLS

The fuel cells are expected for the use in apartment houses, office buildings, and hospitals as several hundreds kW co-generation, in transportations such as automobiles and buses as power sources, in households as several kW power sources, and in electronic devices as several 10 W power sources such as laptops, mobile phones, portable power tools, smoke detectors and burglar alarms (Hoogers, 2003).

1.4. TYPES OF FUEL CELLS

There are different types of fuel cells such as alkaline fuel cells, phosphoric acid fuel cells (PAFCs), polymer electrolyte membrane fuel cells (PEMs), molten carbonate fuel cells (MCFCs), solid oxide fuel cells (SOFCs), direct methanol fuel cells (DMFC). The kind of electrolyte, operating temperature, system output, electrical efficiency, applications, advantages and disadvantages are given in Table 1.1.

Table 1.1. Currently developed types of fuel cells and their characteristics and applications.

Fuel Cell Type	Common Electrolyte	Operating Temperature	System Output	Efficiency Electrical	Applications	Advantages	Disadvantages
Polymer Electrolyte Membrane (PEM)*	Solid organic polymer poly-perfluorosulfonic acid	50 - 100°C 122 - 212°F	<1kW - 250kW	53-58% (transportation) 25-35% (stationary)	•Backup power •Portable power •Small distributed generation •Transportation	•Solid electrolyte reduces corrosion & electrolyte management problems •Low temperature •Quick start-up	•Requires expensive catalysts •High sensitivity to fuel impurities •Low temperature waste heat •Waste heat temperature not suitable for combined heat and power (CHP)
Alkaline (AFC)	Aqueous solution of potassium hydroxide soaked in a matrix	90 - 100°C 194 - 212°F	10kW - 100kW	60%	•Military •Space	•Cathode reaction faster in alkaline electrolyte, higher performance	•Expensive removal of CO from fuel and air streams required (CO degrades the lectrolyte)
Phosphoric Acid (PAFC)	Liquid phosphoric acid soaked in a matrix	150 - 200°C 302 - 392°F	50kW – 1MW (250kW module typical)	32-38%	•Distributed generation	•Higher overall efficiency with CHP •Increased tolerance to impurities in hydrogen	•Requires expensive platinum catalysts •Low current and power •Large size/weight
Molten Carbonate (MCFC)	Liquid solution of lithium, sodium, and/or potassium carbonates, soaked in a matrix	600 - 700°C 1112 -1292°F	<1kW – 1MW (250kW module typical)	45-47%	•Electric utility •Large distributed generation	•High efficiency •Fuel flexibility •Can use a variety of catalysts •Suitable for CHP	•High temperature speeds corrosion and breakdown of cell components •Complex electrolyte management •Slow start-up
Solid Oxide (SOFC)	Solid zirconium oxide to which a small amount of Yttria is added	650 - 1000°C 1202 -1832°F	5kW - 3MW	35-43%	•Auxiliary power •Electric utility •Large distributed generation	•High efficiency •Fuel flexibility •Can use a variety of catalysts •Solid electrolyte reduces electrolyte management problems	•High temperature enhances corrosion and breakdown of cell components •Slow start-up •Brittleness of ceramic electrolyte with thermal cycling

*Direct Methanol Fuel Cells (DMFC) are a subset of PEM used for small portable power applications with a size range of about a subwatt to 100 W and operating at 60 - 90°

1.5. THE DIRECT METHANOL FUEL CELL

Direct methanol fuel cells (DMFCs) are considered as an attractive alternative compared to other types of fuel cells, because of

1) the readily availability of methanol,

2) the potentially, high energy content per mass unit (Liebhavskky and Cairns, 1968; Cathro and Weeks, 1971).

3) the existence of methanol in the liquid phase at room temperature (Mcnicol, 1981)

4) the lack of sulfur and nitrogen additives in the fuel which would produce byproducts, such as SO_2 and NO_x, during the oxidation reaction. CO_2 is the only by-product of the reaction.

Direct methanol fuel cells have been considered for use in transportation applications due to low complexity, high efficieny, cleanliness of the system and wide availability of the methanol. When providing current, methanol is electrochemically oxidized at the anode electrocatalyst to produce electrons which travel through the external circuit to the cathode electrocatalyst where they are consumed together with oxygen in a reduction reaction. The circuit is maintained within the cell by the conduction of protons in the electrolyte. In modern cells, electrolytes based on proton conducting polymer electrolyte membranes (e.g., Nafion™) are often used, since these allow for convenient cell and for high temperature and pressure operation. A schematic description of the components in a DMFC is shown in Figure 1.3. At the anode, methanol is oxidized to carbon dioxide and at the cathode, oxygen is reduced to water (Hamnett et al., 1987). The reactions are:

Anode reaction:

$$CH_3OH + H_2O \rightarrow CO_2 + 6H^+ + 6e^- \qquad E^o = 0.043\ V\ ^* \qquad (vs.\ SHE^\#) \qquad (1.1)$$

Cathode reaction:

$$3/2\ O_2 + 6H^+ + 6e^- \rightarrow 3\ H_2O \qquad E^o = 1.229\ V\ ^* \qquad (vs.\ SHE^\#) \qquad (1.2)$$

Overall reaction:

$$CH_3OH + 3/2\ O_2 \rightarrow CO_2 + 2H_2O \qquad E^o = 1.186\ V\ ^* \qquad (vs.\ SHE^\#) \qquad (1.3)$$

* These are theoretical E^o values calculated from thermodynamic data.

Standart hydrogen electrode.

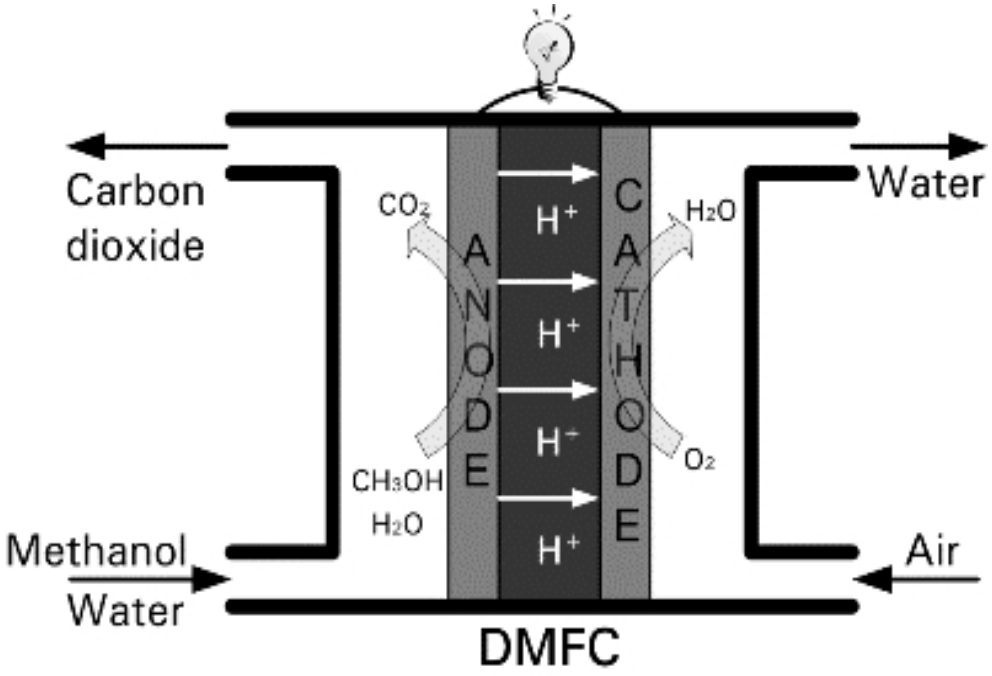

Figure 1.3. Schematic of a DMFC employing an acidic solid polymer electrolyte membrane.

The methanol oxidation reaction may be illustrated as shown in Figure 1.4. In-situ, ex-situ spectroscopic and electroanalytical methods showed that CH_3OH and H_2O (or OH) are adsorbed on the surface of catalyst to produce 3 moles of H^+ and electrons (Weeks, 1988). Then, in order to complete methanol oxidation reaction, oxidation at COH_{ads} occurs via H_2O_{ads} (or OH_{ads}) to form CO_2 and 3 moles of H^+ and electrons. However, methanol oxidation reaction is not as simple as written above, generally adsorbtion of H_2O (or OH) can occur at high potential (>0.5 V) compare to COH adsorption, which cause to flow the other path of the reaction to form bridge and/or linear CO which are called poison (Bagotzky and Vassiliev, 1967; Biegler and Koch, 1967; Bagotzky et al., 1977; Hampson and Willars, 1979; McNicol,1981).

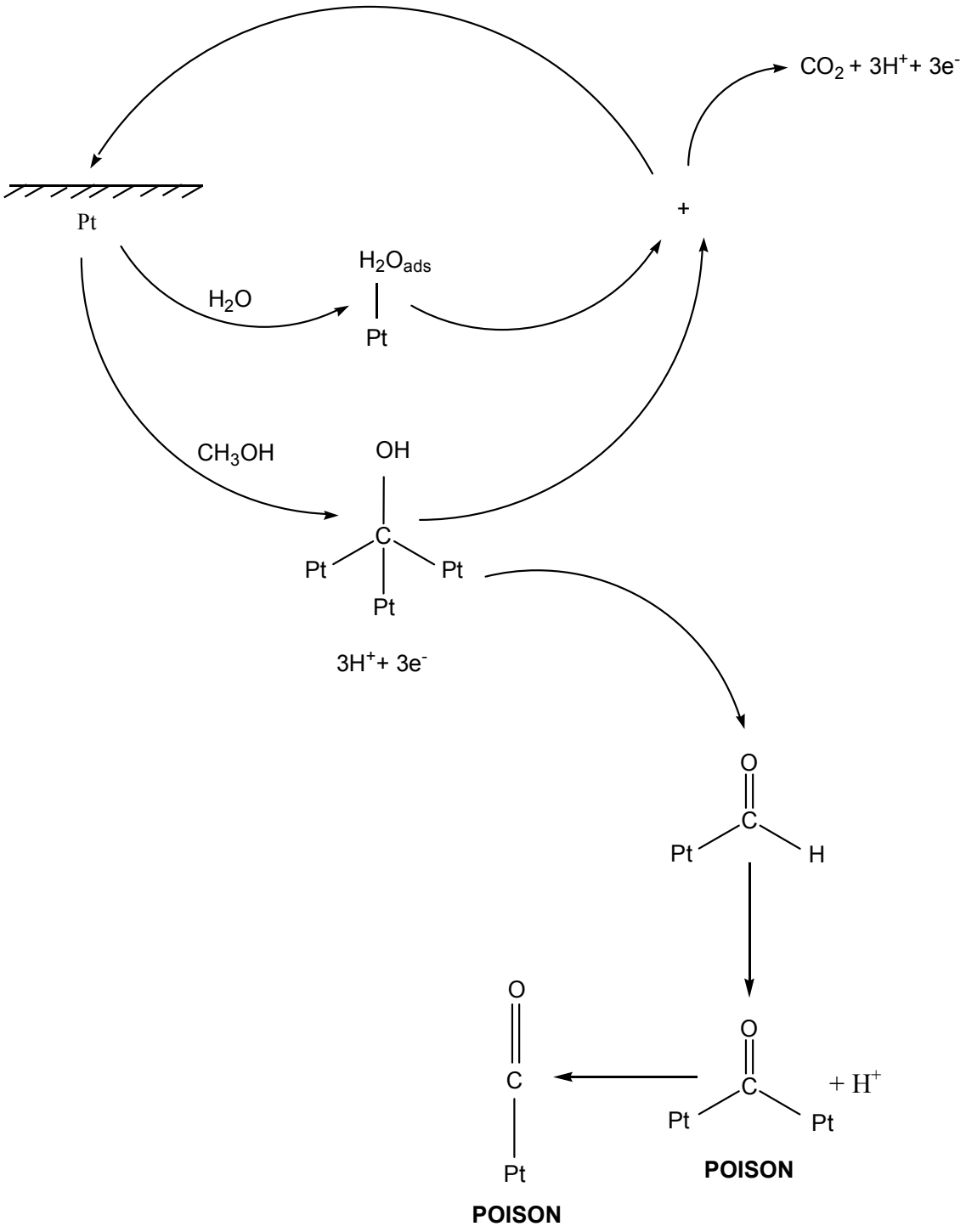

Figure 1.4. Schematic diagram of methanol oxidation occuring on the surface of a platinum catalyst. Two competing reactions occur: oxidation of methanol and the poisoning of the platinum catalyst.

1.5.1. THE NEED FOR A CATALYST

The main problem of using methanol in fuel cells is the poor electrochemical activity of the starting reagent in acidic solution at low potentials. Therefore, a platinum based catalyst especially platinum itself is required to activate the methanol (Bockris and Srinivasan, 1969; McNicol, 1978; Bockris et al., 1981). The development of effective and low cost catalysts for the electro-oxidation of methanol in acidic solution is an essential goal in the development of practical direct methanol-air fuel cells.

1.6. WHAT IS NANOPARTICLES?

A nanoparticle is a microscopic particle with at least one dimension less than 100 nm. Nanoparticle research is currently an area of intense scientific research, due to a wide variety of potential applications in biomedical, optical, and electronic fields. Nanoparticles are of great scientific interest as they are effectively a bridge between bulk materials and atomic or molecular structures. A bulk material should have constant physical properties regardless of its size, but at the nano-scale this is often not the case. Size-dependent properties are observed such as quantum confinement in semiconductor particles, surface plasmon resonance in some metal particles and superparamagnetism in magnetic materials.

The properties of materials change as their size approaches the nanoscale and as the percentage of atoms at the surface of a material becomes significant. For bulk materials larger than one micrometre the percentage of atoms at the surface is minuscule relative to the total number of atoms of the material. The interesting and sometimes unexpected properties of nanoparticles are not partly due to the aspects of the surface of the material dominating the properties instead of the bulk properties. Nanoparticles exhibit a number of special properties relative to bulk material. For example, the bending of bulk copper (wire, ribbon, etc.) occurs with movement of copper atoms/clusters at about the 50 nm scale. Copper nanoparticles smaller than 50 nm are considered super hard materials that do not exhibit the same malleability and

ductility as bulk copper. The change in properties is not always desirable. Ferroelectric materials smaller than 10 nm can switch their magnetisation direction using room temperature thermal energy, thus making them useless for memory storage. Suspensions of nanoparticles are possible because the interaction of the particle surface with the solvent is strong enough to overcome differences in density, which usually result in a material either sinking or floating in a liquid. Nanoparticles often have unexpected visible properties because they are small enough to confine their electrons and produce quantum effects. For example platinum nanoparticles appear deep red to black in solution. Nanoparticles have a very high surface area to volume ratio. This provides a tremendous driving force for diffusion, especially at elevated temperatures. Sintering can take place at lower temperatures, over shorter time scales than for larger particles. This theoretically does not affect the density of the final product, though flow difficulties and the tendency of nanoparticles to agglomerate complicates matters. The surface effects of nanoparticles also reduces the incipient melting temperature (Fiorani, 2005).

1.7. THE AIM OF STUDY

It is well known that the active surface area of solid catalyst is quite important for heterogeneous reaction medium, the greater the active surface area, the greater the activity of the catalyst and as stressed above nanoparticles have a very high ratio of active surface area relative to the total volume. Therefore, in this thesis, carbon supported different size of platinum nanoparticle catalysts have been prepared for oxidation of methanol in acidic medium. $PtCl_4$ and H_2PtCl_6 complexes were used as starting materials and tert-nonyl mercaptane, which was used for the first time in the synthesis of these types of of nanoparticles, 1-heptanethiol, 1-hexadecanethiol and 1-octadecanethiol were utilized as surfactants. The prepared catalysts have been characterized by transmission electron microscopy (TEM), X-ray photoelectron spectroscopy (XPS), X-ray diffraction (XRD) and cyclic voltammetry (CV). The effect of the type of surfactants and starting complexes on the size of platinum nanoparticles has been determined. In addition to these, the activity of the prepared catalysts towards methanol oxidation reaction has been determined by electrochemical studies.

CHAPTER 2

EXPERIMENTAL

2.1. CATALYST PREPARATIONS

2.1.1. PREPARATION OF PLATINUM NANOPARTICLE WITH 1:1 1-HEPTANETHIOL:PLATINUM MOLE RATIO (CATALYST Ia)

0.25 mmol (0.0808g) of $PtCl_4$ (99 %, Alfa) was dissolved in 20 ml of anhydrous tetrahydrofuran (THF, 99.5 %, Merck) for an hour. Then 0.25 mmol (39 μL) of 1-heptanethiol surfactant ($C_7H_{15}SH$, 95 %, Merck) was added to this solution and the mixture was stirred vigorously for 2.5 hours. Finally, thiol stabilized platinum complex was reduced by dropwise addition of lithium triethylborohydride (superhydride, 1.0 M dissolved in THF, Aldrich) until no H_2 gas evolved according to Equation 1. All of these steps were performed under high-purity argon atmosphere. The observation of reddish-brown color of the solution indicated the formation of platinum nanoparticles (Yee et al.1999).

$$PtCl_4\text{-surfactant} + 4LiBEt_3H \rightarrow Pt(\text{nanoparticles})\text{-surfactant} + 4BEt_3 + 4LiCl + 2H_2\uparrow \quad (1)$$

To remove the excess thiols, the resulting solution was washed with 50-60 ml of dry ethanol (99.9 %, Merck) in an ultrasonic bath and then the solution was centrifuged for an hour to have most of the particles precipitated (Brust et al., 1994). This process was continued until a clear filtrate solution was obtained. Finally, the solid residue was dried under vacuum at room temperature.

2.1.2. PREPARATION OF OTHER PLATINUM NANOPARTICLE CATALYSTS WITH 1:1 SURFACTANT/PLATINUM MOLE RATIO

Appropriate amount of $PtCl_4$ or H_2PtCl_6 was used as starting materials for the preparation of Catalyst Ia, IIa, IIIa, IVa and Catalyst Ib, IIb, IIIb, IVb. 1-Heptanethiol, tert nonyl mercaptan, 1-hexadecanethiol, 1-octadecanethiol were used as surfactants for Catalyst I a-b, Catalyst II a-b, Catalyst III a-b and Catalyst IV a-b, respectively, and the same procedure was followed as in Section 2.1.1 (Table 2.1.).

Table 2.1. Platinum complexes and surfactants used for Catalysts Ia-IVa and Catalysts Ib-IVb

Catalyst	Platinum Compd.	Surfactant
Catalyst Ia	$PtCl_4$	1-Heptanethiol
Catalyst Ib	H_2PtCl_6	1-Heptanethiol
Catalyst IIa	$PtCl_4$	Tert Nonyl Mercaptan
Catalyst IIb	H_2PtCl_6	Tert Nonyl Mercaptan
Catalyst IIIa	$PtCl_4$	1-Hexadecanethiol
Catalyst IIIb	H_2PtCl_6	1-Hexadecanethiol
Catalyst IVa	$PtCl_4$	1-Octadecanethiol
Catalyst IVb	H_2PtCl_6	1-Octadecanethiol

2.1.3. PREPARATION OF CARBON SUPPORTED PLATINUM NANOPARTICLE CATALYSTS

The prepared Pt nanoparticles were mixed in a 1:10 ratio with carbon XC-72 (Liu et al., 2004) which is used as a support. 10 ml of dry ethanol was added to the mixture and it was stirred vigorously for three days in order to obtain uniform distribution of

metal nanoparticles on carbon support. Then, the slurry mixture was dried at room temperature under vacuum.

2.2. ELECTRODE PREPARATION

A mixture of 36.78 mg of prepared carbon supported Pt powder catalyst, 0.5 mL of Nafion (Aldrich, 5 wt %), 0.15 mL of N,N-dimethyl formamide (Merck, 99.5 %) and 2.5 mL of distilled water was sonicated until almost homogenous dispersion of solid in solution was obtained. 50 µL of the slurry solution was dropped on a 0.7 cm-diameter glassy carbon, which was used as a working electrode. Then, the electrode was dried at 40^{o}C for 20 minutes, 65^{o}C for 20 minutes and 100^{o}C for an hour in order to get good adhesion. (Gökağaç et al., 2001).

2.3. DETERMINATION OF PLATINUM CONTENT IN THE PREPARED CATALYSTS

100 ml of aqua regia (the mixture of 3 volumes of HCl (37 %, Merck) and 1 volume of concentrated HNO_3 (65 %, Merck)) was added to the certain amount of prepared catalyst and the mixture was evaporated until the volume decreased to 25 mL. Then 25 ml of concentrated HCl was added to this solution and heated up until almost all the solvent was evaporated. This process was repeated 4 times. Later, the resulting solution was filtered and diluted to 100 ml with distilled H_2O. Finally, ICP measurements were done by Leeman Lab ICP instrument at METU Central Lab. to determine the amount of platinum in the prepared catalyst.

2.4. PHYSICAL TECHNIQUES

2.4.1. CYCLIC VOLTAMMETRY

Cyclic voltammetry measurements are performed by applying a triangular potential waveform to the working electrode as shown in Figure 2.1.

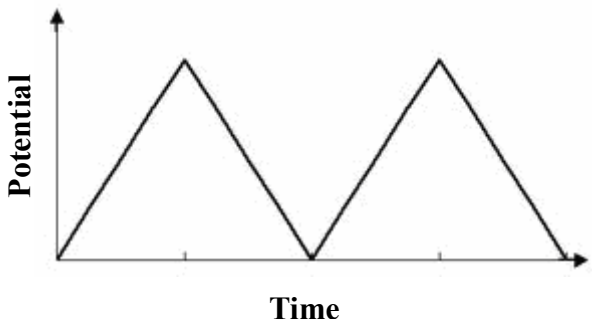

Figure 2.1. Cyclic Voltammetry waveform

In a typical cyclic voltammetry, a solution component is electrolyzed (oxidized or reduced) by placing the solution in contact with an electrode surface, and then making that surface sufficiently positive or negative in voltage to force electron transfer. In simple cases, the surface is started at a particular voltage with respect to a reference half-cell such as calomel or Ag/AgCl, the electrode voltage is changed to a higher or lower voltage at a linear rate, and finally, the voltage is changed back to the original value at the same linear rate. When the surface becomes sufficiently negative or positive, a solution species may gain electrons from the surface or transfer electrons to the surface. This results in a measurable current in the electrode circuitry. When the voltage cycle is reversed, it is often the case that electron transfer between electrode and chemical species will also be reversed, leading to an "inverse" current peak. These features are illustrated in Figure 2.2.

The potential difference between the reduction and oxidation peaks is theoretically 59 mV for a reversible reaction. In practice, the difference is typically 70-100 mV. Larger differences, or nonsymmetric reduction and oxidation peaks are an indication of a nonreversible reaction. These parameters of cyclic voltammograms make CV most suitable for characterization and mechanistic studies of redox reactions at electrodes.

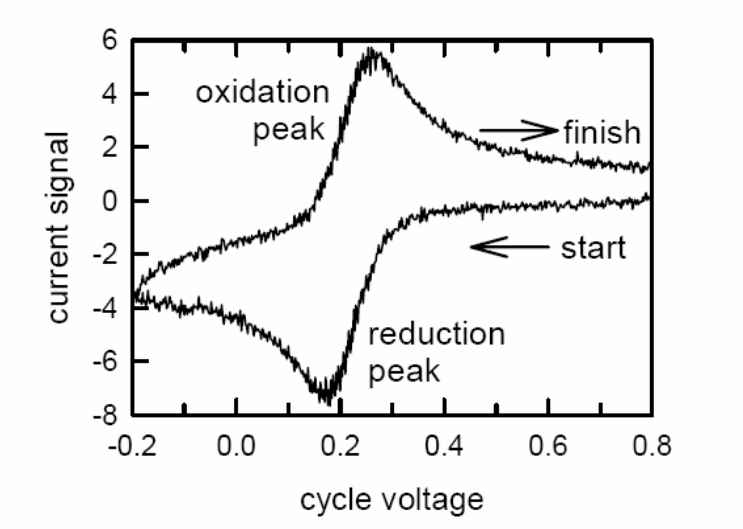

Figure 2.2. A typical cyclic voltammogram showing reduction and oxidation current peaks.

2.4.1.1. ELECTROCHEMICAL CELL DESIGN

The cyclic voltammetry measurements were performed with a conventional three electrode configuration using a microcomputer-controlled potentiostat/galvanostat (Solartron 1285) (in the Chemistry Department of METU) at room temperature, Figure 2.3. The working electrode was made of prepared catalysts settled on a 0.7 cm diameter glassy carbon. Saturated calomel electrode (SCE) and glassy carbon were used as the reference and counter electrodes, respectively. 0.1 M $HClO_4$ (60 %, Merck) or 0.1 M $HClO_4$ + 0.4 M CH_3OH (99.8 %, Merck) solutions were used as an electrolyte. Pure Ar gas was purged through electrolyte for at least 15 minutes prior to each experiment in order to remove oxygen in the electrolyte and electrochemical cell.

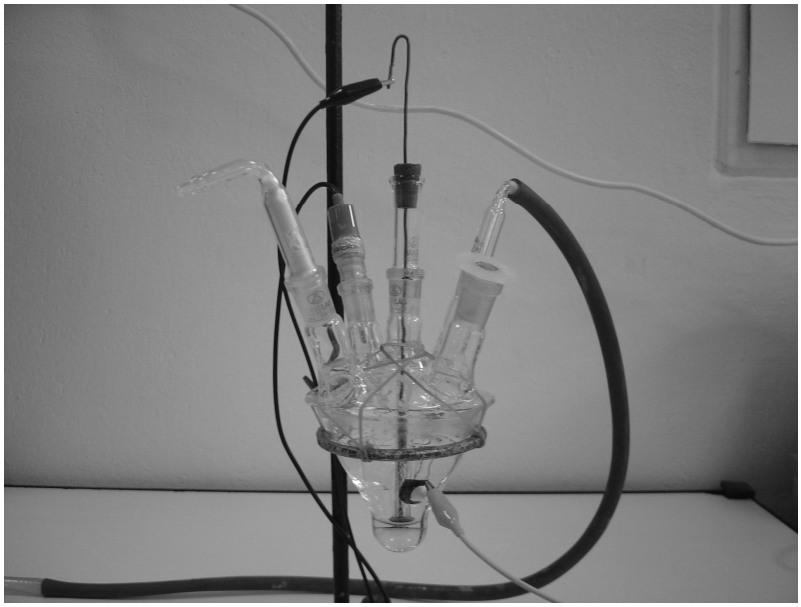

Figure 2.3. An electrochemical cell.

2.4.2. X-RAY DIFFRACTION

X-ray diffraction has been in use in two main areas, for the fingerprint characterization of crystalline materials and the determination of their structure. Each crystalline solid has its unique characteristic X-ray powder pattern which may be used as a "fingerprint" for its identification. Once the material has been identified, X-ray crystallography may be used to determine its structure, i.e. how the atoms pack together in the crystalline state and what the interatomic distance and angle are etc. X-ray diffraction is one of the most important characterization tools used in solid state chemistry and materials science.

W.L. Bragg (early 1900's) showed that diffracted X-rays act as if they were "reflected" from a family of planes within crystals. Bragg's planes are the rows of atoms that make up the crystal structure (Kinoshita and Stoneheart, 1977).

These "reflections" were shown to only occur under certain conditions which satisfy the equation:

$$n\lambda = 2\ d\ \mathrm{Sin}\theta \text{ (Bragg Equation)}$$

where n is an integer (1, 2, 3, ..., n); λ is the wavelength; d is the distance between atomic planes; and θ is the angle of incidence of the X-ray beam and the atomic planes. 2dSinθ is the path length difference between two incident X-ray beams where one X-ray beam takes a longer (but parallel) path because it "reflects" off an adjacent atomic plane. This path length difference must equal an integer value of the λ of the incident X-ray beams for constructive interference to occur such that a reinforced diffracted beam is produced, Figure. 2.4.

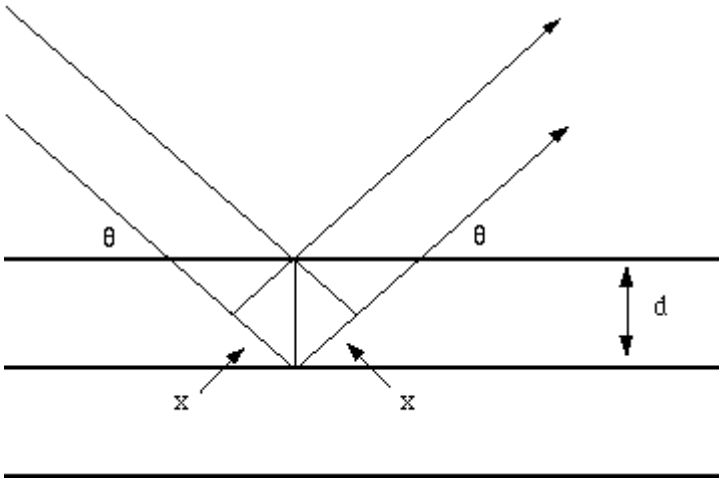

Figure 2.4. The path of X-rays.

There are two main techniques for X-ray diffraction. These are:

(i) Single-Crystal Method: (X-ray beam is focused on a single crystal).

In a single crystal setup, an X-ray detector is mounted as shown in Figure 2.5. A mechanical device keeps the detector oriented so that the angle of incidence equals the angle of reflection for the desired crystal plane. Peaks in the X-ray detection rate are sought as the angle θ is varied.

The advantage of this type of apparatus is that diffraction peaks from only the selected crystal plane are observed.

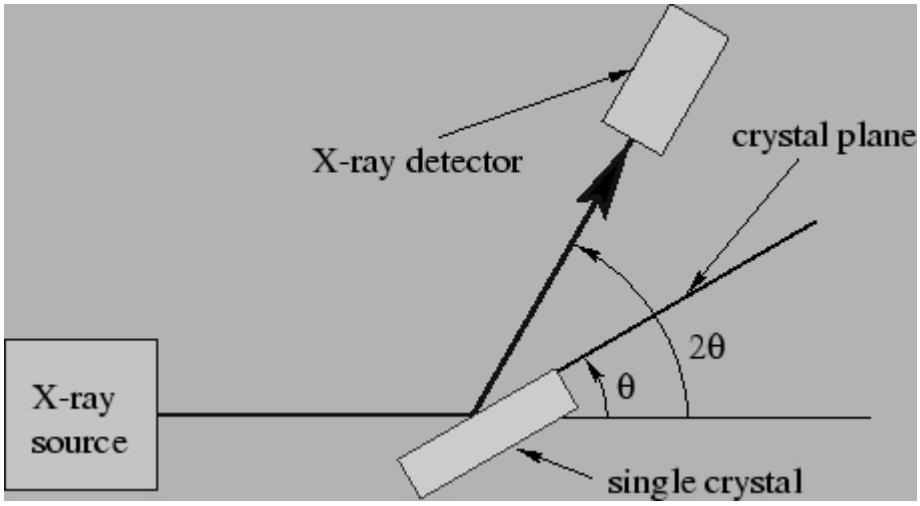

Figure 2.5. Setup for single crystal Bragg diffraction.

(ii) Powder Method: (X-ray beam focused on a powder pellet or powder smeared on a glass slide).

The powder in a powder target is really a conglomeration of many tiny crystals randomly oriented. Thus, for each possible Bragg diffraction angle there are crystals oriented correctly for Bragg diffraction to take place. The detector is usually a photographic plate or an equivalent electronic device as illustrated in Figure 2.6. For each Bragg diffraction angle one sees a ring on the plate concentric with the axis of the incident X-ray beam.

The advantage of this type of system is that no a prior knowledge is needed of the crystal plane orientations. Furthermore, a single large crystal is not required. However, all possible Bragg scattering angles are seen at once, which can lead to confusion in the interpretation of the results.

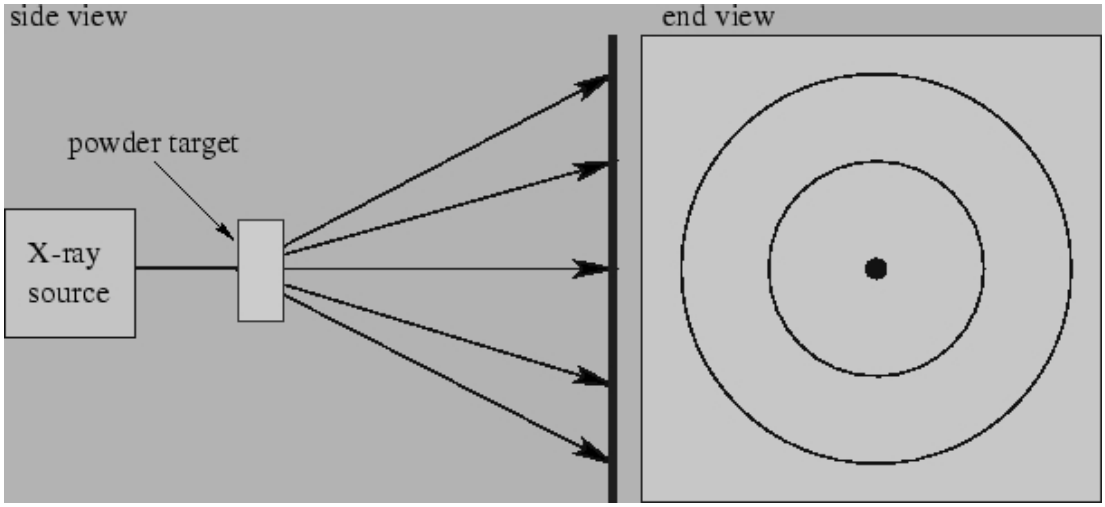

Figure 2.6. Setup for powder target Bragg diffraction.

In this study, synthesized Pt nanoparticle catalyst particle sizes were calculated from X-ray diffraction pattern using line broadening of the peaks according to the Scherrer formula (Kinoshita and Stoneheart, 1977);

$L = k\lambda / (\beta_{1/2} \text{Cos}\theta)$

where $\beta_{1/2}$ is the breadth of a diffraction peak at half-height, measured in radians, λ is the wavelength of the incident X-rays, L is the effective crystallite diameter, θ is the position of the peak maximum and k is a constant [taken to be 0.9 as recommended by Klug and Alexander (1962)]. X-ray powder diffraction (XRD) patterns were taken by using Rigaku Miniflex diffractometer with Ultima + theta-theta high resolution goniometer and Cu (Kα, 30 kV, 15 mA, λ = 1.54056Å) radiation in Chemistry Department at METU. (Scan range: $5° < 2\theta < 100°$, sampling width: 0.05 deg./step, scan speed: 1.000 deg./min.)

2.4.3. TRANSMISSION ELECTRON MICROSCOPY

The transmission electron microscope is an optical analogue to the conventional light microscope. It is based on the fact that electrons can be ascribed a wavelength (of the order of 2.5 pm) but at the same time interact with magnetic fields as a point charge.

A beam of electrons is applied instead of light, and the glass lenses are replaced by magnetic lenses. The lateral resolution of the best microscopes are down to atomic resolution.

A schematic presentation of the microscope is shown in Figure 2.7. With an electron gun (not shown), an electron beam is formed, which is accelerated by an electric field formed by a voltage difference of, typically, 200 kV. By condensor lenses, the electron beam is focused to a spot of the order of 1 mm on the thin film to be investigated. The first image, which is formed by the objective lens, is magnified

typically 25 times, and the following lenses give a final magnification of the image of more than 10^6.

In addition to thin-sample images, electron diffraction patterns can also be formed on the final image screen. The electron rays corresponding to bright field imaging and (selected area) diffraction are shown in the left and right drawings of Figure 2.7, respectively. In bright field imaging, the image of a thin sample is formed by the electrons that pass the film without diffraction, the diffracted electrons being stopped by a diaphragm. In the corresponding dark field imaging mode, a diffracted beam is used for imaging.

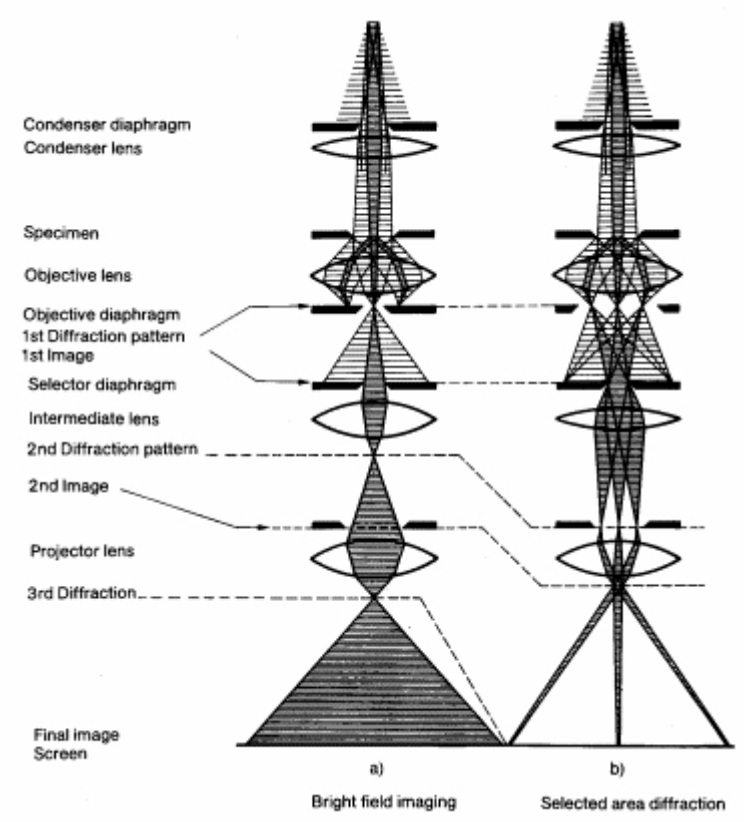

Figure 2.7. Schematic presentation of a transmission electron microscope.

The microstructure, e.g. the grain size, and lattice defects are studied by use of the image mode, while the crystalline structure is studied by the diffraction mode.

In addition, the chemical composition of small volumes, for example grain boundaries, can be obtained by detection of X-rays emitted from the film.

Samples for electron microscopy in form of films mounted on fine-meshed grids are required to be very thin. In case near-atomic resolution is required film thicknesses have to be limited to a few tens of Å. Therefore, the quality of the electron microscopy work is sometimes limited by the thinning-down procedure as structural changes may occur during the thinning.

There are a number of drawbacks to the TEM technique. Many materials require extensive sample preparation to produce a sample thin enough to be electron transparent, which makes TEM analysis a relatively time consuming process with a low throughput of samples. The structure of the sample may also be changed during the preparation process. Also the field of view is relatively small, raising the possibility that the region analysed may not be characteristic of the whole sample. There is potential that the sample may be damaged by the electron beam, particularly in the case of biological materials (Williams and Carter, 1996).

In this study, transmission emission micrographs of carbon supported Pt nanoparticle catalysts were taken by Jeol JEM 3010, 300 kV (at Kırıkkale University). Sample preparation for TEM involves dispersion of the carbon supported material in carbon tetrachloride using an ultrasonic bath. This solution was then dropped onto a 400 mesh copper grid and left to dry at room temperature.

2.4.4. X-RAY PHOTOELECTRON SPECTROSCOPY

X-ray Photoelectron Spectroscopy (XPS) is a quantitative spectroscopic technique that measures the empirical formula, chemical state and electronic state of the elements that exist within a material. XPS requires ultra-high vacuum (UHV) conditions.

XPS is a surface chemical analysis technique that can be used to analyze the chemistry of the surface of a material in its "as received" state, or after some treatment such as: fracturing, cutting or scraping in air or UHV to expose the bulk chemistry, ion beam etching to clean off some of the surface contamination, exposure to heat to study the changes due to heating, exposure to reactive gases or solutions, exposure to ion beam implant, exposure to UV light, for example.

XPS detects all elements with an atomic number (Z) between those of lithium (Z=3) and lawrencium (Z=103). This limitation means that it cannot detect hydrogen (Z=1) or helium (Z=2). Detection limits for most of the elements are in the parts-per-thousand (ppt) range. XPS is routinely used to analyze inorganic compounds, metal alloys, semiconductors, polymers, pure elements, catalysts, glasses, ceramics, paints, papers, inks, woods, plant parts, make-up, teeth, bones, human implants, bio-materials, viscous oils, glues, ion modified materials and many others.

XPS spectra are obtained by irradiating a material with a beam of X-rays while simultaneously measuring the kinetic energy (KE) and number of electrons that escape from the top 1 to 10 nm of the material being analyzed by using an equation that is based on the work of Ernest Rutherford (1914):

$$E_{\text{binding}} = E_{\text{photon}} - E_{\text{kinetic}} - \Phi$$

where E_{binding} is the energy of the electron emitted from one electron configuration within the atom, E_{photon} is the energy of the X-ray photons being used, E_{kinetic} is the kinetic energy of the emitted electron as measured by the instrument and Φ is the work function of the material (Figure 2.8). Because the energy of a particular X-ray wavelength equals a known quantity, we can determine the electron binding energy (BE) of each of the emitted electrons.

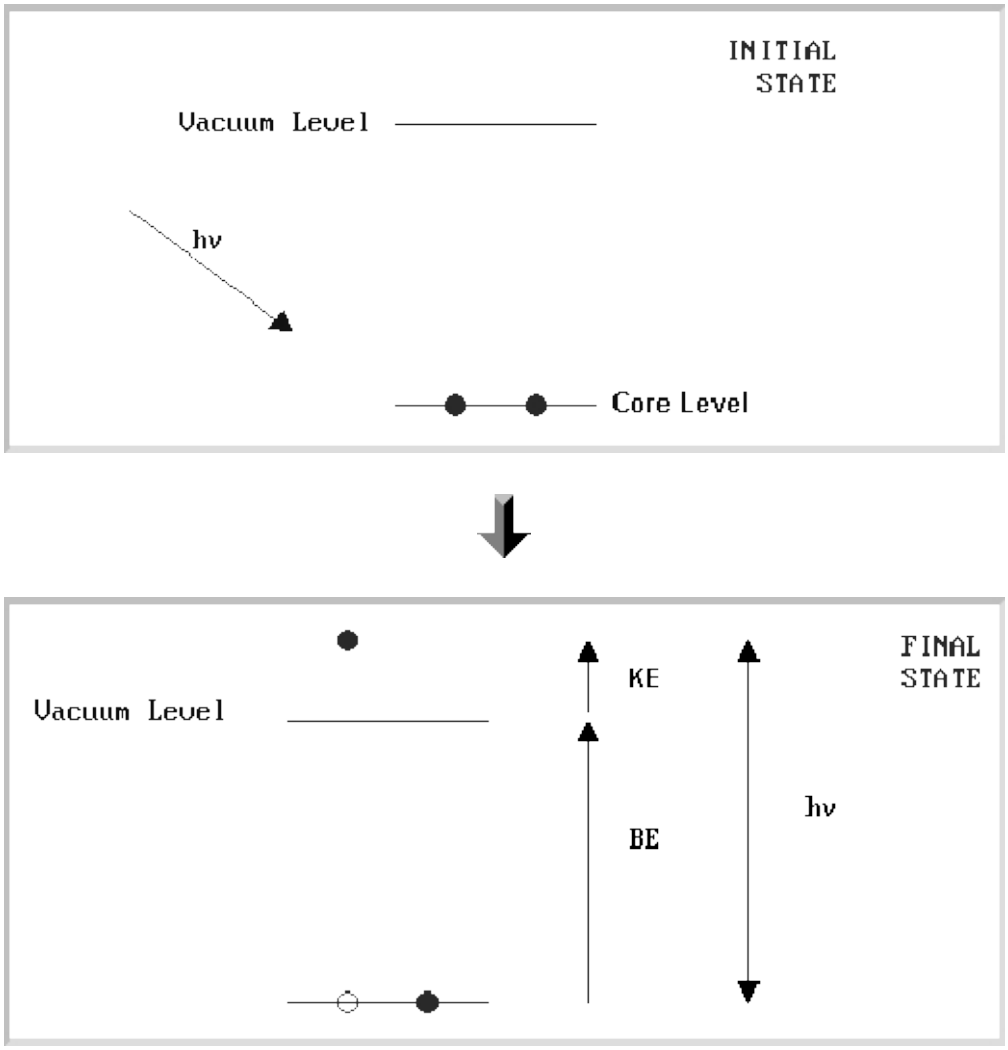

Figure 2.8. The energies of electrons ejected from core levels in X-ray photoelectron spectroscopy (XPS).

In this study, the binding energies of Pt $4f_{7/2}$ and $4f_{5/2}$ electrons were determined for all prepared catalysts by Specs spectrometer using Kα lines of Mg (1253.6 eV, 10 mA) as a X-ray source at Central Labortory of METU. The spectrometer has two stainless steel chambers with independent pumping systems. The first chamber is a fast entry lock working between 10^{-4}-10^{-5} torr. The second chamber operates between 10^{-9}-10^{-10} torr and is used to remove high volatile gases.

The second chamber is the main chamber where the spectroscopic values are taken by a hemispherical analyser with a multichannel detector. The Ar^+ ion flood was used to clean the surface when necessary. Samples were held in a copper holder with double-sided tape.

All lines were referenced to the C 1s line at 284.5 eV. Peak fittings of Pt $4f_{7/2}$ - $4f_{5/2}$ regions of nanoparticle catalysts were done using peak fitting programme (Briggs and Seah, 1983; Nefedov, 1988).

CHAPTER 3

RESULTS AND DISCUSSION

3.1. X-RAY DIFFRACTION AND TRANSMISSION ELECTRON MICROSCOPY

The average crystallite particle sizes of all prepared catalysts were determined by both X-ray diffraction and transmission electron microscopy. The average particle size of the crystallite species was estimated from powder X-ray diffraction pattern using the line broadening of the peaks according to the Scherrer formula (Kinoshita and Stoneheart, 1977);

$$L = k\lambda/(\beta_{1/2}\text{Cos}\theta)$$

where L is effective crystalline diameter, k is constant taken to be 0.9 as recommended by Klug and Alexander (Klug and Alexander, 1962), λ is the wavelength of the incident X-rays, $\beta_{1/2}$ is the breadth of a diffraction peak at half-height (measured in radians) and θ is the position of the peak maximum. It should be noted that line broadening can also arise from crystallite imperfections along with the instrumental factors which causes a conservatively estimated error of ±20 % (Weeks, 1988). Whilst such line broadening is useful in determining the average particle size in systems with a narrow particle size distribution, it is of limited value where a wide range of particle sizes and/or morphologies are present, and in general will overestimate the particle size. Electron microscopy enables the direct observation of individual crystallites and provides that sufficient care is taken, can give both the average particle size and the size distribution.

When taken together, diffraction studies and analytical electron microscopy are a powerful approach in characterizing supported metallic crystallites.

The powder diffraction patterns of all catalysts showed broad peaks at about 2θ = 39.90 (1 1 1), 46.35 (2 0 0) and 67.75 (2 2 0) (JCPDS Card No: 87-0640), which correspond to the face-centered cubic structure of platinum (Sen and Gokagac, 2007), Figure 3.1. The line broadening was a result of the small size of the particles. Additional very sharp peaks were also observed in the diffraction pattern at about 2θ = 21.40, 23.40, 30.70, 31.55, 33.90, 36.20 and 37.00. It is believed that these peaks might be due to some kind of crystalline form of sulphur hydrocarbon compound (one of the possibilities which was found using Rigaku XRD programme is $CS(HS)_2$) or residue which could not be removed during the cleaning process.

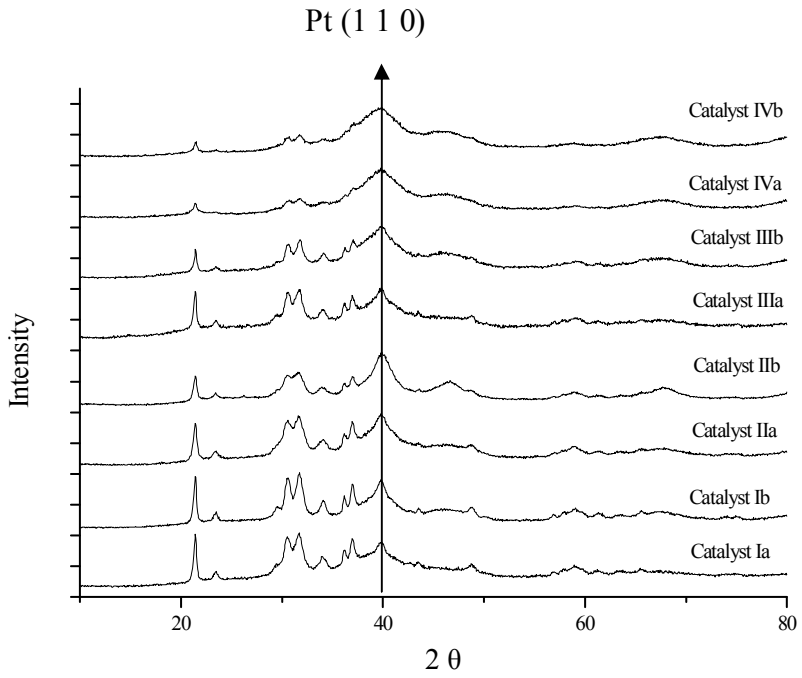

Figure 3.1. X-ray diffractograms of all prepared catalysts.

Using X-ray diffraction pattern, the average particle size of platinum was found to be ~2.0 nm, ~3.0 nm, ~1.2 nm and ~1.0 nm for Catalysts I a-b, Catalysts II a-b, Catalysts III a-b and Catalysts IV a-b, respectively, Table 3.1. These results showed

that the size of crystalline platinum nanoparticles is not dependent on the type of precursor platinum compounds, but surfactants. The average platinum particle size of Catalysts II a-b (~3.0 nm) was larger than that of Catalysts I a-b (~2.0 nm), as observed in the previous study (Sen and Gokagac, 2007). In that study, it has been reported that the size of the platinum particles were about 2 nm when 1-hexanethiol was used as a surfactant, and $PtCl_4$ and H_2PtCl_6 were used as a starting materials, on the other hand, the platinum nanoparticle sizes were found to be about 3 nm when tert-octanethiol was used as a surfactant. Therefore, it is thought that an increase in particle size of platinum nanoparticles was most probably due to the branched structure of the tert-octanethiol and tert-nonyl mercaptane. A more branched surfactant may have a tendency to form a larger hole in the micelles, which in turn would cause an increase in the particle size of the metal which forms in the cavity of the micelles (Sen and Gokagac, 2007). A schematic of this is represented in Figure 3.2. The other point that should be stressed here is the chain length of surfactant, as the length of chain increase the size of platinum crystallites decreases as reported in references (Tu et al., 2003).

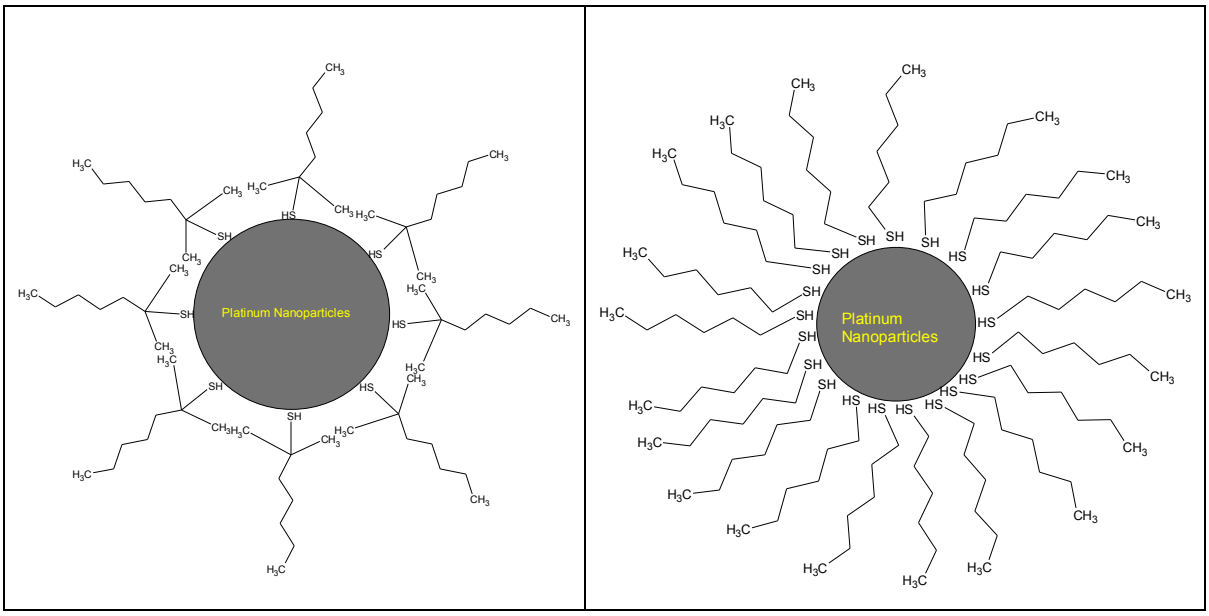

Figure 3.2. Schematic representation of formation of the platinum nanoparticles.

An electron micrograph and histogram of the platinum particle size distribution of Catalysts Ia and IIa are shown in Figures 3.3.a.b. A relatively narrow range of platinum particle sizes and uniform distribution of those nanoparticles on carbon support was observed by transmission electron microscopy. The average particle size was found to be ~2.0 ± 0.2 nm for Catalyst I a-b, ~3.0 ± 0.2 nm for Catalyst II a-b, ~1.2 ± 0.2 nm for Catalysts III a-b and ~1.0 ± 0.2 nm for Catalyst IV a-b, Table 3.1. These results are in agreement with the X-ray diffraction data. In all cases, there is no evidence of agglomeration of the platinum nanoparticles.

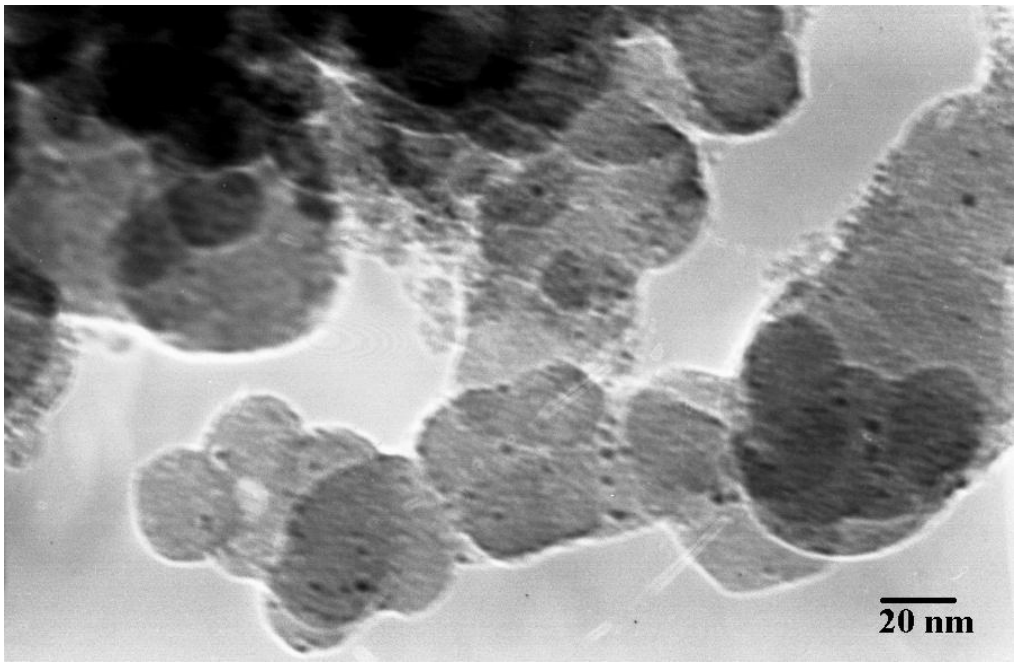

Figure 3.3.a. Transmission electron micrograph and histogram of the platinum particle size distribution of Catalyst Ia.

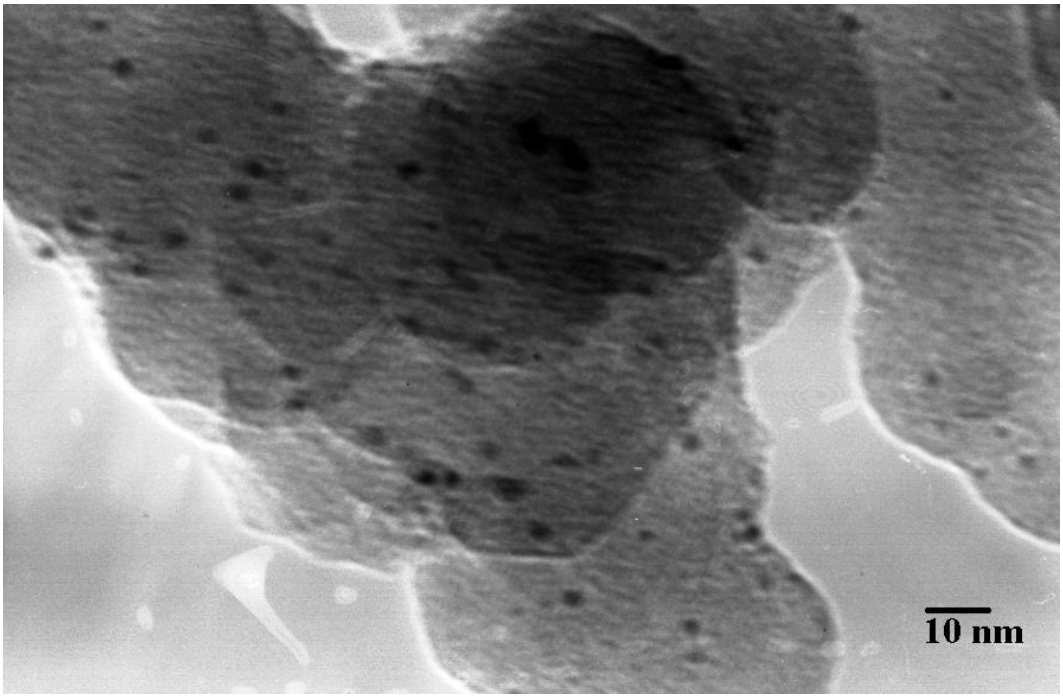

Figure 3.3.b. Transmission electron micrograph and histogram of the platinum particle size distribution of Catalyst IIa.

Table 3.1. Average crystallite platinum particles size determined by (a) X-ray line broadening and (b) transmission electron microscopy

Catalysts	a	b
Catalysts Ia	~2.0 nm	~2.0 ± 0.2 nm
Catalysts Ib	~2.0 nm	~2.0 ± 0.2 nm
Catalysts IIa	~3.0 nm	~3.0 ± 0.2 nm
Catalysts IIb	~3.0 nm	~3.0 ± 0.2 nm
Catalysts IIIa	~1.2 nm	~1.2 ± 0.2 nm
Catalysts IIIb	~1.2 nm	~1.2 ± 0.2 nm
Catalysts IVa	~1.0 nm	~1.0 ± 0.2 nm
Catalysts IVb	~1.0 nm	~1.0 ± 0.2 nm

3.2. X-RAY PHOTOELECTRON SPECTROSCOPY

The composition, environment and relative surface concentrations of all prepared catalysts have been investigated by X-ray photoelectron spectroscopy. In all cases, Pt 4f, S 2p, O 1s and C 1s spectra were recorded and survey spectra showed platinum, sulfur and oxygen signals as well as strong C signal, Figure 3.4. The existence of carbon peak, with the C 1s binding energy, E_b, of 284.5 eV, indicates the presence of carbon in all catalysts so that the surfactants can not be removed even on extensive washing. The O 1s region of the spectra of all prepared catalysts showed a symmetric peak near 532.0 eV, Figure 3.5.a, b and Table 3.2. The Gaussian curve fitting analysis for O 1s electron spectra of all catalysts indicated a single peak between 531.7 and 532.5 eV with a half with of about 1.6 eV, except Catalyst IIa and b. While a single O 1s peak was observed at 533.2 eV for catalyst IIa, a double O 1s peaks were observed at 532.4 eV (65%) and 534.5 eV (35%) for catalyst IIb. Previous works have shown that binding energies for oxides and adsorbed oxygen are both about 530.0 ± 0.5 eV, while adsorbed hydroxide on platinum occurs at about 531.5 ± 0.5 eV. The O 1s level for adsorbed water is around 533.0 ± 1.0 eV (Peuckert, 1984; Peuckert et al., 1984). Thus, it can be concluded that all of the prepared catalysts surface contain adsorbed hydroxide and no significant variation between the various samples observed, but Catalyst IIa, where adsorption of water was detected, and Catalyst IIb, where adsorption of 65 % of hydroxide and 35 % of water were identified.

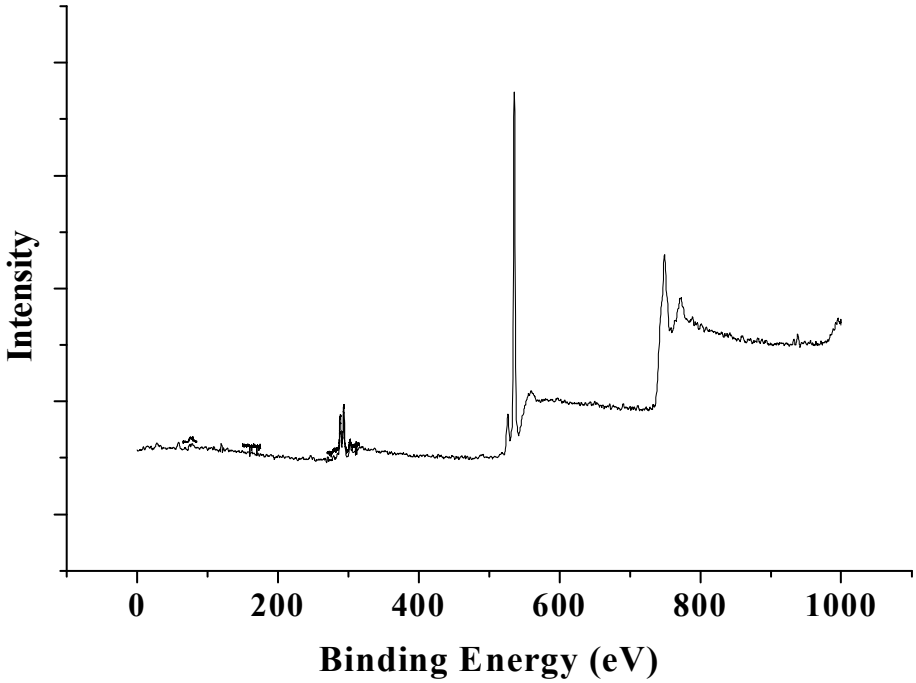

Figure 3.4. Wide range X-ray photoelectron spectra of a Catalyst Ia.

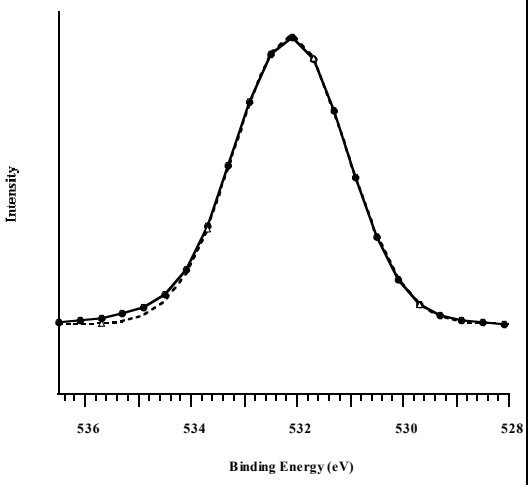

Catalyst Ia
(O 1s region)

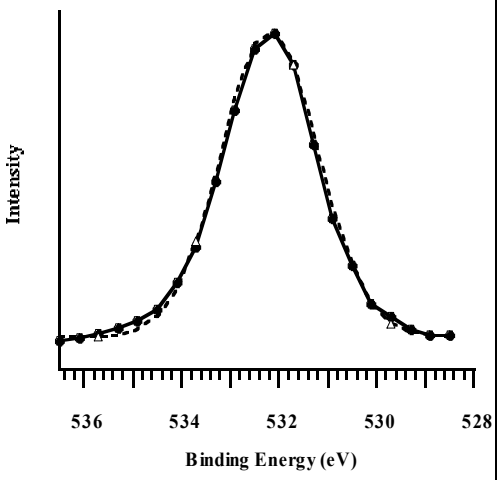

Catalyst Ib

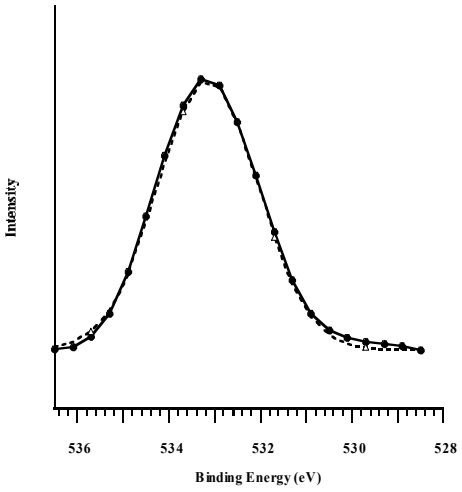

Catalyst IIa

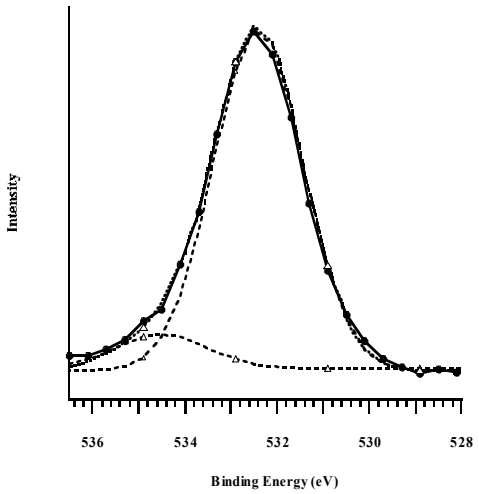

Catalyst IIb

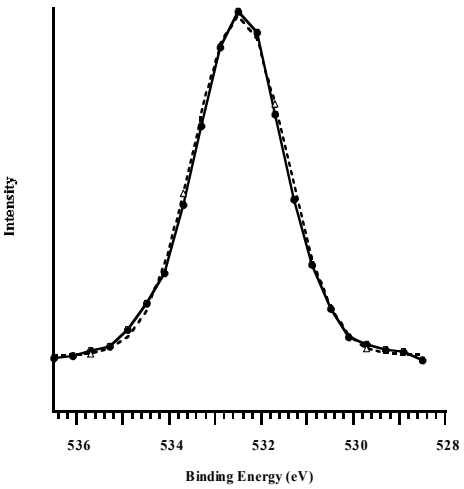

Catalyst IIIa

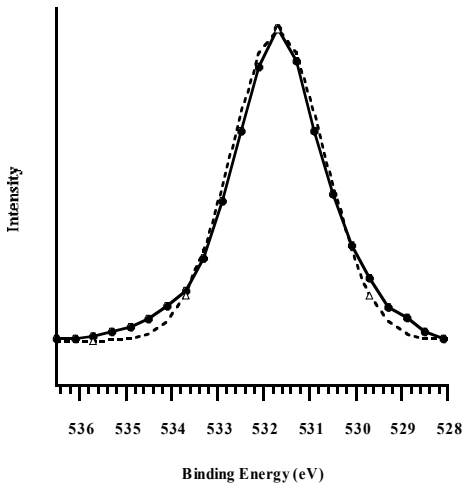

Catalyst IIIb

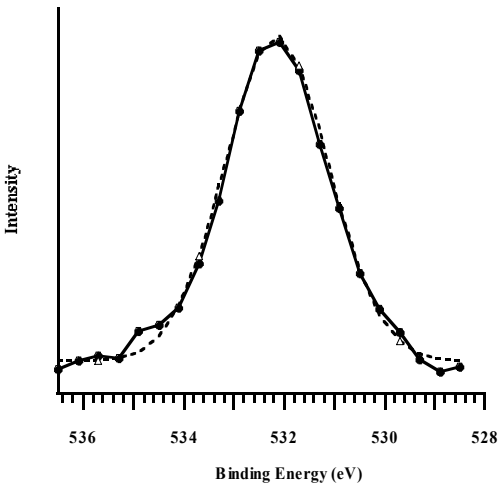

Catalyst IVa

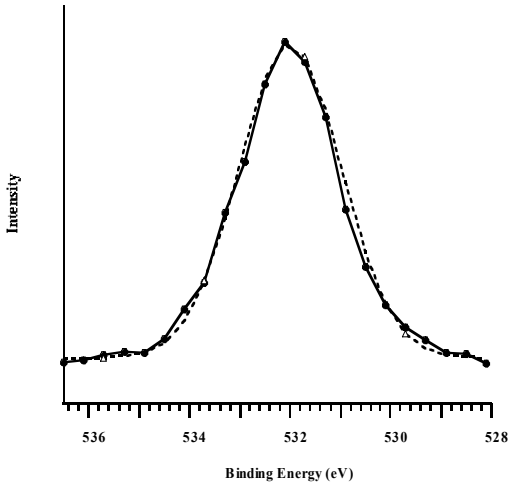

Catalyst IVb

Figure 3.5. O 1s electron spectra of all the catalysts

Table 3.2. O 1s core binding energies, eV, in the prepared catalysts. The number in the parentheses is the relative intensities of the species.

	O 1s	O 1s
Catalysts	Adsorbed hydroxide	Adsorbed water
Catalysts Ia ($PtCl_4$+1-Heptanethiol)	532.1	
Catalysts Ib (H_2PtCl_6+1-Heptanethiol)	532.2	
Catalysts IIa ($PtCl_4$+Tert Nonyl Mercaptan)		533.2
Catalysts IIb (H_2PtCl_6+Tert Nonyl M ercaptan)	532.4 (65)	534.5 (35)
Catalysts IIIa ($PtCl_4$+1-Hexadecanethiol)	532.5	
Catalysts IIIb (H_2PtCl_6+1-Hexadecanethiol)	531.7	
Catalysts IVa ($PtCl_4$+1-Octadecanethiol)	532.2	
Catalysts IVb (H_2PtCl_6+1-Octadecanethiol)	532.0	

The S 2p region of XPS was evaluated for all catalysts. It was found that all catalysts contain sulfur peak but Catalysts IIa and b, indicating the absence of sulfur in these catalyst. All spectra could be fitted using a 2:1 peak area ratio and a 1.2 eV splitting (Castner, 1996), as shown for Catalyst I a in Figure 3.6. The S 2p spectrum has two doublets, which indicates the presence of two kinds of sulfur. The first doublet with a binding energy of the S $2p_{3/2}$ peak is between 162.0 eV and 162.7 eV, Table 3.3, indicating that a sulfur atom bound to the platinum surface as a thiolate species as reported by Castner for thiols bound on a gold surface (Castner, 1996). The second doublet with a binding energy of S $2p_{3/2}$ is between 164.0 eV and 165.5 eV and is due to unbound thiol, or disulfide within or on top of the thiolate adlayer as reported by Zubraegel et. al. (Zubraegel et al.). These results also show the presence of sulfur containing sample on the surface of the platinum nanoparticles for all catalysts except Catalyst IIa and IIb.

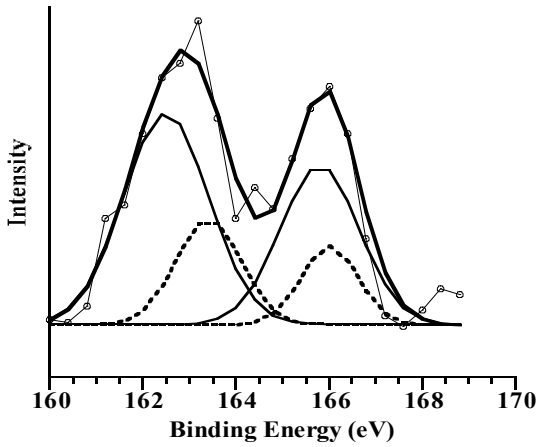

Catalyst Ia (S 2p region)

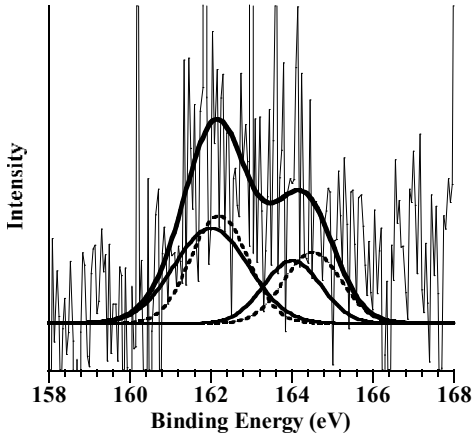

Catalyst Ib

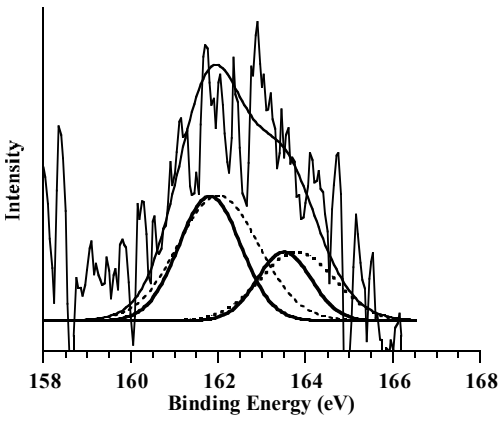

Catalyst IIIa

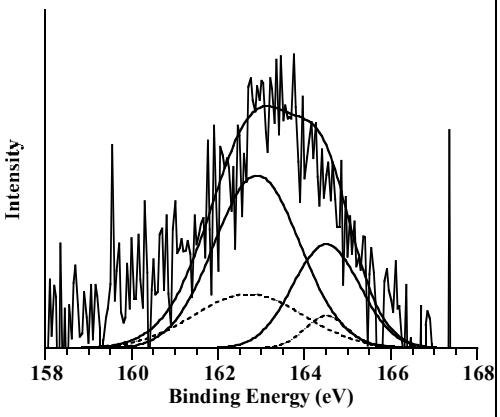

Catalyst IIIb

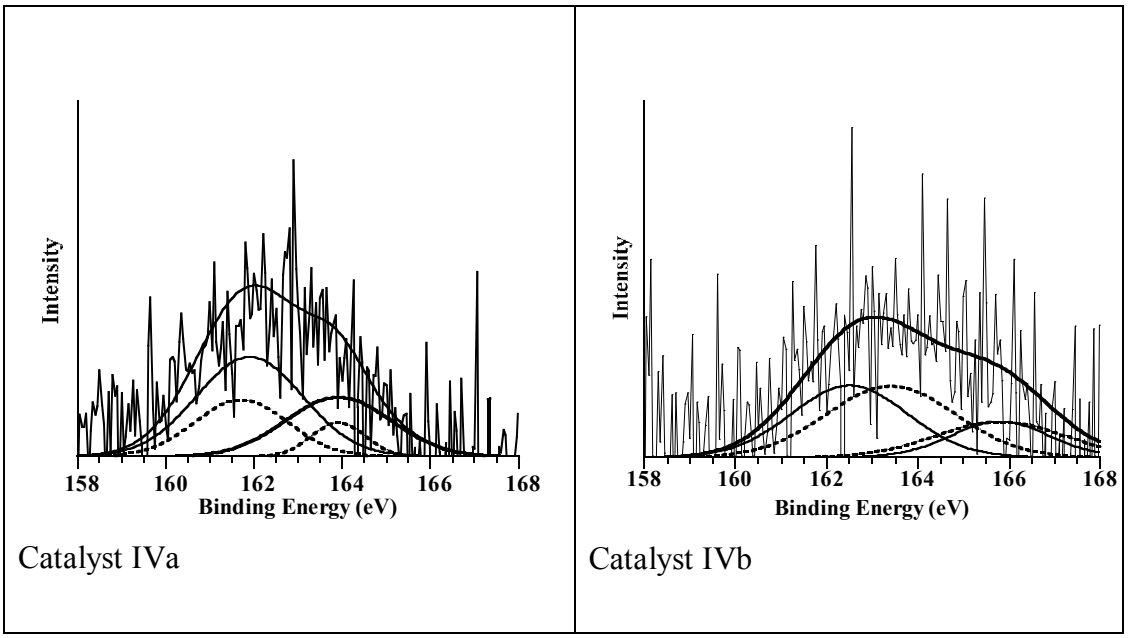

Figure 3.6. S 2p electron spectra of all catalysts.

Table 3.3. S $2p_{3/2}$ core binding energies, eV, in the prepared catalysts. The number in the parentheses is the relative intensities of the species.

	S $2p_{3/2}$	S $2p_{3/2}$	
Catalysts	Bounded Thiols	Unbonded thiols	Ratio (B/U)
Catalyst Ia	162.4	165.5	1.46
Catalyst Ib	162.2	164.5	1.70
Catalyst IIIa	162.1	164.0	2.02
Catalyst IIIb	162.7	164.5	2.48
Catalyst IVa	162.0	164.0	1.94
Catalyst IVb	162.4	165.5	2.17

The Pt 4f electron spectra are shown in Figure 3.7 and the results are summarized in Table 3.4.

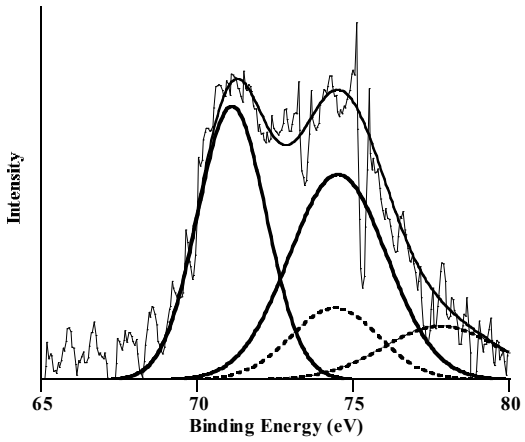

Catalysts Ia (Pt 4f region)

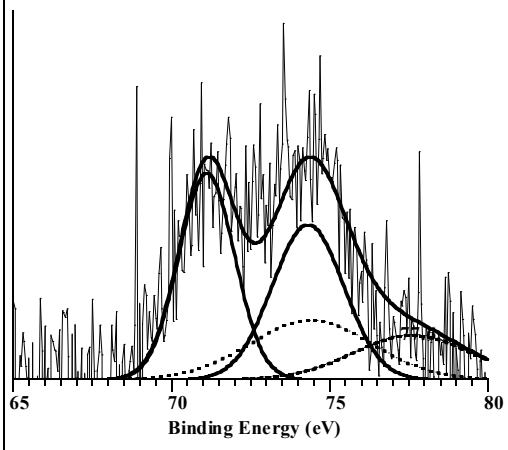

Catalysts Ib

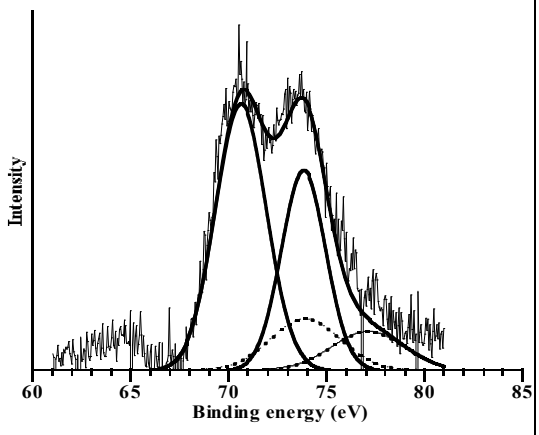

Catalysts IIa

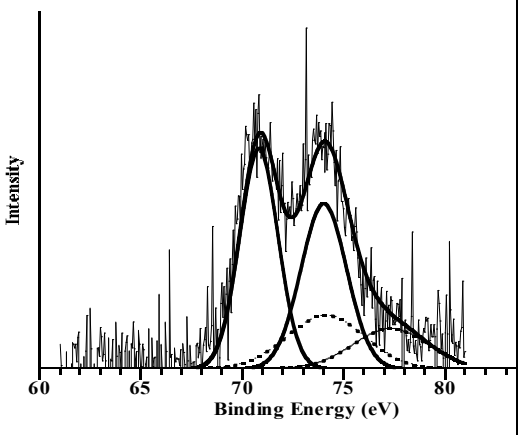

Catalysts IIb

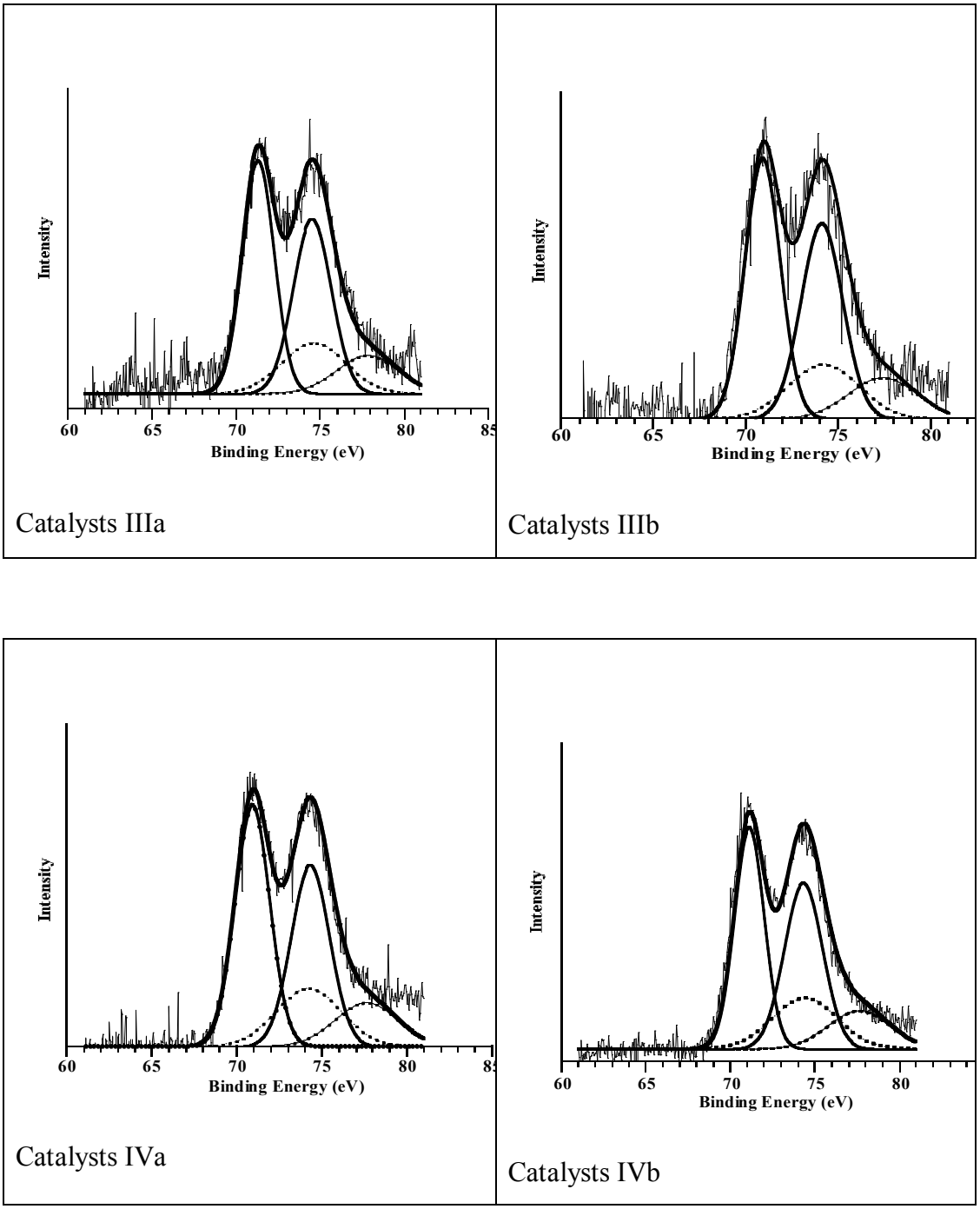

Figure 3.7. Pt 4f electron spectra of all prepared catalysts

In fitting of the spectrum to a series of Gaussion lines, which have almost equal half-widths with an intensity ratio of ca. 3:4 and a separation of about 3.35 eV, shows the prepared catalysts to consist of two platinum species. In all cases, the Pt 4f lines were well resolved $4f_{7/2}$ and $4f_{5/2}$ two doublets with Pt $4f_{7/2}$ binding energies of 70.6 – 71.2 and 73.9 – 74.7 eV. The line at 70.6 – 71.2 eV is unquestionably due to Pt(0) (Gokagac, 1993), while the line at 73.9 – 74.7 eV, is most probably because of the presence of Pt(IV) species such as PtO_2 and/or $Pt(OH)_4$. Previous studies indicate that the Pt $4f_{7/2}$ was at 74.4 eV for $Pt(OH)_4$ (Goodenough et al, 1988) and it was between 74.6 and 74.9 eV for PtO_2 (Watanabe et al, 1987).

It is well known that XPS enables quantification of the various oxidation states of a particular element present in the sample besides the identification of the surface species. In general, the Pt(0)/Pt(IV) ratio was observed between 65-78/35-22. Individual investigation among the XPS data showed that, Pt(0) to Pt(IV) ratio is larger for the Catalysts Ia and IIa where $PtCl_4$ was used as a precursor and they have higher activity toward methanol oxidation reaction, compare to the Catalysts Ib and IIb where H_2PtCl_6 was used as a precursor. The same trend, however, was not observed for the other catalysts, indicating that it is unclear what should be the optimum Pt(0)/Pt(IV) ratio in catalyzing the methanol oxidation reaction, because XPS is an ex-situ techniques, therefore, it is not possible to predict the Pt(0)/Pt(IV) ratio on the surface of the catalyst during the methanol oxidation reaction. However comparing the Pt 4f and O 1s region of X-ray photoelectron spectra might give us an important clue on the performance of catalysts towards methanol oxidation reaction. As can be seen in the cyclic voltammetry section, Catalyst IIa is the most active catalyst towards methanol oxidation reaction. That catalyst has a Pt 4f peak at lower binding energy values (70.6 eV (78%)) which indicates high electron density around platinum metal atoms compared to the others and the same catalyst revealed presence of O 1s peak at higher binding energy values which display the adsorption of water (at 533.2 eV) instead of hydroxide on the surface of catalyst. These results might show that adsorbed water and platinum metal with a high electron density are the most convenient medium for the adsorption and oxidation of methanol on the surface of catalyst.

Table 3.4. Pt $4f_{7/2}$ core binding energies, eV, in the prepared catalysts. The number in the parentheses is the relative intensities of the species.

	Pt $4f_{7/2}$	Pt $4f_{7/2}$
Catalysts	Pt(0)	Pt(IV)
Catalysts Ia	71.1 (76)	74.7 (24)
Catalysts Ib	71.0 (65)	74.4 (35)
Catalysts IIa	70.6 (78)	73.9 (22)
Catalysts IIb	70.8 (69)	74.1 (31)
Catalysts IIIa	71.2 (72)	74.5 (28)
Catalysts IIIb	70.9 (73)	74.3 (27)
Catalysts IVa	70.9 (71)	74.2 (29)
Catalysts IVb	71.1 (70)	74.4 (30)

3.3. CYCLIC VOLTAMMETRY

It is well known that cyclic voltammetry provide information about electrochemical reactivity and stability of an electrode. Therefore, cyclic voltammograms of the prepared catalyst were recorded both in 0.1 M $HClO_4$ and 0.1 M $HClO_4$ + O.5 M CH_3OH. Although small shift in the position of some of the peaks were noted, the cyclic voltammograms of all catalysts in 0.1 M $HClO_4$ are similar and typical example is shown in Figure 3.8. The voltammograms consist of hydrogen adsorption/desorption (left of the cyclic voltammogram) and oxygen adsorption/desorption (right of the voltammogram) regions. Hydrogen reduction starts at about -0.32 V and follows a rapid increase in cathodic current due to bulk H_2 evolution.

$$2H^+ + 2e^- \rightarrow H_2(g)$$

On the reverse scan, oxidation of hydrogen was observed in the cathodic region.

$$H_2(g) \rightarrow 2H^+ + 2e^-$$

In the anodic sweep, adsorption of water and oxidation of platinum involves at least three steps:

$$Pt + H_2O \rightarrow Pt\text{-}(OH)_{ads} + H^+ + e^-$$

$$Pt(OH)_{ads} \rightarrow PtO_{ads} + H^+ + e^-$$

$$PtO_{ads} \rightarrow Pt\text{-}O$$

The adsorption of water on platinum appears as a shoulder at lower potential while the formation of bulk platinum oxide ($Pt\text{-}O_{ads}$) is observed at more positive potentials in the cyclic voltammogram. In the cathodic scan, the reduction of platinum oxides was observed at about +0.5 V and the reaction is given below:

$$Pt\text{-}O + 2H^+ + 2e^- \rightarrow Pt + H_2O$$

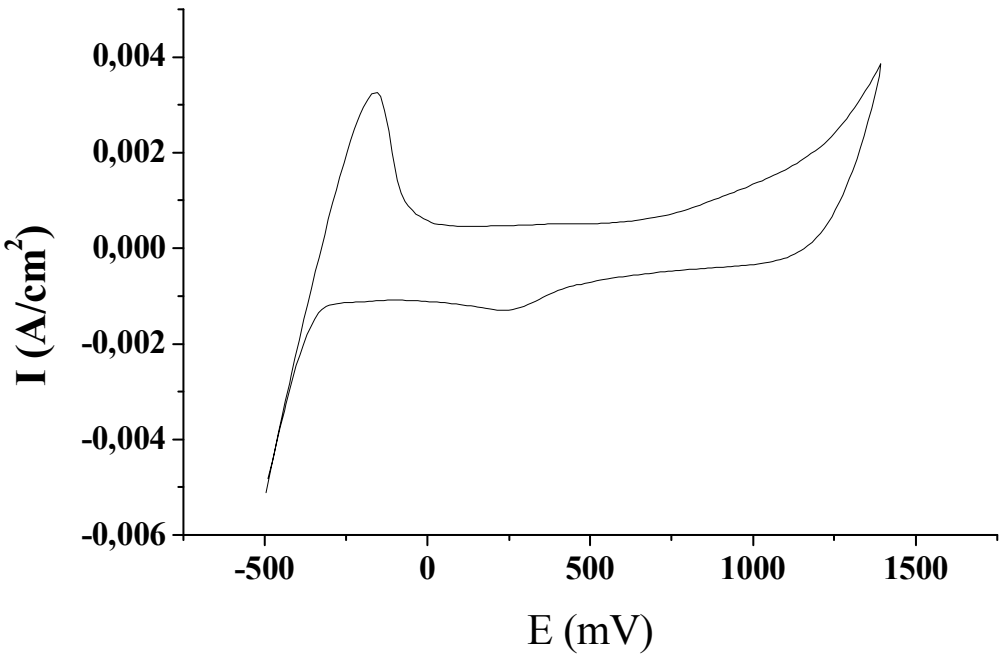

Figure 3.8. Cyclic voltammogram of Catalyst Ia in 0.1 M $HClO_4$ at room temperature. Scan rate is 50 mV/s.

A dramatic change in the appearance of the cyclic voltammograms was observed after the addition of methanol to the 0.1 M $HClO_4$ electrolyte. The cyclic voltammograms of all catalyst exhibit a "classical" methanol oxidation response, Figure 3.9. Methanol oxidation reaction commences at about 0.3 V on the anodic sweep and above ~0.65 V it is prevented by platinum oxide formation and anodic current decreases until the potential is swept into the oxygen evolution region. On the reverse scan, after reduction of platinum oxide from the surface of catalyst, methanol oxidation recommences around 0.55 V and becomes cathodic at about 0.45 V, corresponding to hydrogen adsorption region.

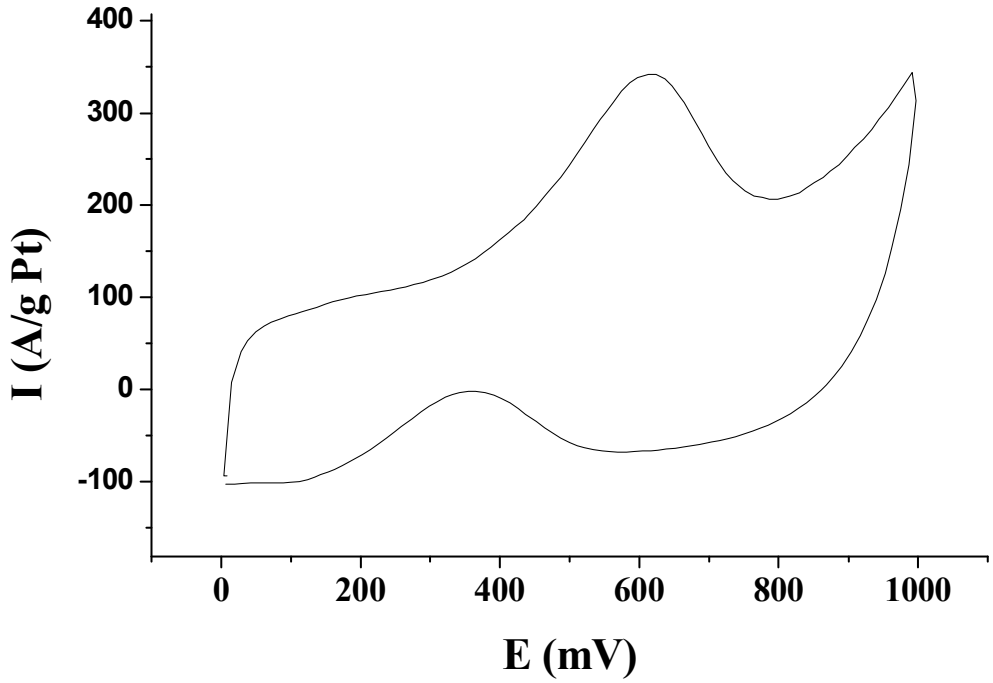

Figure 3.9. Cyclic voltammogram of Catalyst IIa in 0.1 M $HClO_4$ + 0.5 M CH_3OH at room temperature. Scan rate is 50 mV/s.

Only the anodic part of the cyclic voltammograms of all catalysts is shown in Figure 3.10 to compare the activity of catalyst towards methanol oxidation reaction. The cyclic voltammograms showed that catalyst IIa has the maximum activity (~342 A / g Pt at 0.612 V) while Catalysts IIIb has the least active one (~91 A / g Pt at 0.580 V). It is possible to classify the prepared catalysts in two groups: Group A, where $PtCl_4$ was used as a precursor; and Group B, where H_2PtCl_6 was used as a precursor. Within the same group, the Catalysts Ia-IVa have higher catalytic activity towards methanol oxidation reaction or methanol oxidation reaction starts at lower potential compared to the Catalysts Ib-IVb. It is also possible to classify the prepared catalyst according to the surfactants, for instance, Group C which prepared by using a linear surfactant (1-heptanethiol, hexadecanethiol and octadecanethiol) and a branch surfactant (tert-nonyl mercaptan) was utilized for Group D. Group D catalyst showed higher activity, however, methanol oxidation reaction peak was at higher potentials compared to Group C. These results might exhibit the importance of particle size of platinum nanoparticles as well as the oxidation state of platinum, their ratios and adsorbed species on the surface of catalysts and so on. As given in reference (Sen and Gokagac, 2007), the optimum platinum nanoparticle size for methanol oxidation reaction could be about 3.0 nm and the performance of catalyst is decreased as the particle size of platinum is decreased (Sen and Gokagac, 2007).

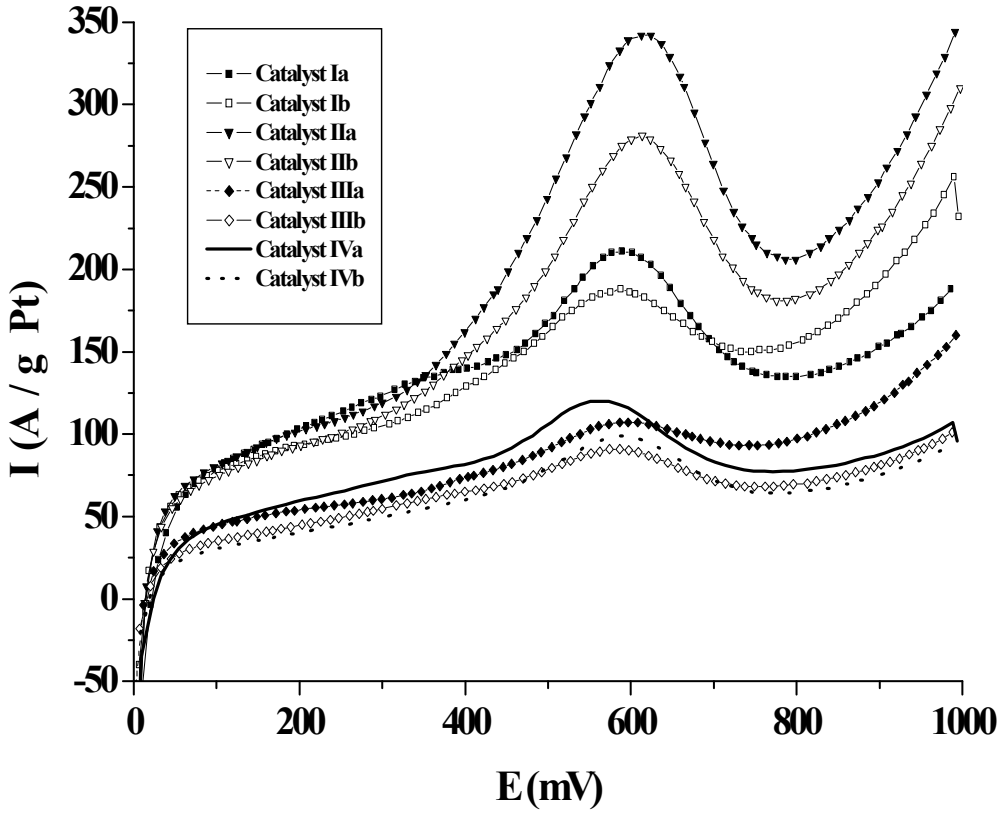

Figure 3.10. Anodic part of the cyclic voltammogram of Catalyst Ia in 0.1 M $HClO_4$ + 0.5 M CH_3OH at room temperature. Scan rate is 50 mV/s.

As given in the introduction section (Figure 1.4), spectroscopic and electrochemical studies indicated that methanol oxidation reaction is achieved by first adsorption of methanol and H_2O (or OH) on the surface of catalysts, COH_{ads} and H_2O_{ads} or OH_{ads}, by giving 3 moles of electrons and H^+, and then oxidation of COH_{ads} via H_2O_{ads} (or OH_{ads}) to form 3 moles of electrons and H^+, and a mole of CO_2 which is the one of the main product of methanol oxidation reaction. The point that should be stressed here is the adsorption potential value of COH_{ads} and H_2O_{ads} (or OH_{ads}). It has been shown that while COH_{ads} occurs at low potentials (about 0.2 V), H_2O_{ads} (or OH_{ads}) forms at high potentials (> 0.5V). Consequently, scientists have been trying to find a catalyst which can produce H_2O_{ads} (or OH_{ads}) at low potentials as COH_{ads}.

As given in the last step of the mechanism, oxidation of COH_{ads} could be realized by either H_2O_{ads} or OH_{ads}, which is not clearly given in the literature, because the separation of these two adsorbed species is quite difficult with today's techniques. Therefore, it might be speculative, however our experimental results indicated that an increase in the amount of adsorbed H_2O on the surface of catalysts causes an increment in the rate of oxidation of COH_{ads} to CO_2. Therefore, Catalysts IIa and b, where adsorbed water was observed, are more active compared to the other prepared catalysts.

The other parameter on the activity of catalysts is the particle size of the platinum nanoparticles. As can be seen in the mechanism, in order to get those adsorbed species on the surface of the platinum, a sufficient surface area is needed. Consequently, it is thought that the optimum size for platinum nanoparticles to catalyze the methanol oxidation reaction is about 3 nm, which was observed for Catalyst IIa and IIb.

In addition to these, the sulfur content of the catalyst is also play a noteworthy factor on the performance of the prepared catalysts. For example, the Catalysts II a and b, which do not contain sulfur, are quite active towards the desired reaction. Under these circumstances, it is possible to say that, in addition to above reasons, absence of sulfur in the catalyst cause an enlargement of the active surface area of the catalysts, which enhance the activity of catalysts towards methanol oxidation reaction.

As stressed above, there are two types of sulfur atom on the surface of all catalysts except Catalyts IIa and b. One of them is the bound thiol to the platinum surface and the other one is the unbound thiol.

Bound to unbound thiol ratio is smaller for Catalyts Ia, IIIa and IVa compared to Catalyts Ib, IIIb and IVb, respectively (Table 3.3), and the activity of Catalyts Ia, IIIa and IVa is larger than Catalyts Ib, IIIb and IVb. Besides this, Catalysts IIIa, IIIb, IVa and IVb have high bound to unbound thiol ratios and they have lower activity towards methanol oxidation reaction compared to the other prepared catalysts.

All these results indicated that presence of sulfur especially bound sulfur decrease the active surface area of the catalysts that cause decline of activity of catalysts.

CHAPTER 4

CONCLUSIONS

Using different starting metal complexes, $PtCl_4$ and H_2PtCl_6, and surfactants, 1-heptanethiol, tert-nonyl mercaptane, heptadecanethiol and octadecanethiol, carbon supported platinum nanoparticle catalysts were prepared, analyzed and used for methanol oxidation reaction which is the anodic compartment reaction for direct methanol fuel cells. The surfactant tert-nonyl mercaptane was used for the first time in this type of catalyst preparation and the other surfactants were used for comparison of the catalysts performance. The following results were found, these are:

a) The structure of surfactant has an effect on the size of platinum nanoparticles, such as branch surfactant, tert-nonyl mercaptane, causes an increase in the size of platinum nanoparticles compared to linear surfactant, 1-heptanethiol, as observed for tert-octanethiol surfactant.
b) Increase in the ratio of bonded to unbound sulfur in thiolate species on the platinum nanoparticles decrease the activity of catalysts toward methanol oxidation reaction.
c) The optimum platinum nanoparticle size is about 3 nm and the Pt(0) to Pt(IV) ratio is about 7.5 to 2.5 toward methanol oxidation reaction among the prepared catalysts.
d) Adsorption of water instead of hydroxide on the surface of catalysts increases the activity of catalysts toward methanol oxidation reaction.

REFERENCES

Bacon, F.T., Chapter 5, ed. Young, G.J., *Fuel Cells, Vol.1, Reinhold Publishing Corporation,* New York, 1960.

Bagotzky, V.S. and Vassiliev, Yu.B., *Electrochimica Acta*, 12, 1323, 1967.

Bagotzky, V.S., Vassiliev, Yu.B., and Khazova, O.A., *Journal of Electroanalytical Chemistry*, 81, 229, 1977.

Bauer, E. and Ehrenberg, H., *Zeitschrift für Electrochemie*, 18, 1002, 1912.

Biegler, T. and Koch, D.F.A., *Journal of the Electrochemical Society*, 114, 904, 1967.

Bockris, J.O'M. and Srinivasan, S., *Fuel Cells – Their Electrochemistry*, McGraw Hill, New York, 1969.

Briggs, D and Seah, M.P., *Practical Surface Analysis, Vol. 1, Auger and X-Ray Photoelectron Spectroscopy*, John Wiley and sons Ltd, U.K., 1983.

Brust, M., Walker, M., Bethell, D., Schiffrin, D.J., and Whyman, R., *Journal of the Chemical Society, Chemical Communications*, 801, 1994.

Castner, D.G., *Langmuir*, 12, 5083, 1996.

Cathro, K.J. and Weeks C.H., *Energy Conversion*, 11, 143, 1971.

Cohn, E.M., Fuel Cell Systems, ed. R.F. Gould, *Advances in Chemistry Series, 47, American Chemical Society,* Washington D.C., 1965.

Fiorani, D. (Ed.), Surface Effects in Magnetic Nanoparticles, XIV, 300 p., Hardcover, ISBN: 978-0-387-23279-9, 2005.

Goodenough, J.B., Hamnett, A., Kennedy, B.J., Manoharan, R., and Weeks, S.A., *Journal of Electroanalytical Chemistry*, 240, 133, 1988.

Gökağaç, G., Metal Oxides as Promoters for Methanol Oxidation, Doctor of Philosophy Thesis in Chemistry, Univerity of Sydney, Australia, 1993a.

Gökağaç, G., Leger, J.M., and Hahn, F., *Z. Naturforsch*, 56 b, 1306, 2001.

Grove, W.R., *Philosophical Magazine and Journal of Science*, 14, 127, 1839.

Grubb, W.T. and Niedrach, L.W., *J. Electrochem. Soc.,* 112, 117, 1960.

Haber, F. and Moser, A., *Zeitschrift für Elektrotechnik und Electrochemie*, 11, 593, 1905.

Hamnett, A., Christensen, P.A., Kennedy, B.J., and Weeks, S.A., *E.E.C. Periodic Report*, Dec., 1987.

Hampson, N.A. and Willars, M.J., *Journal of Power Sources*, 4, 191, 1979.

Hoogers, G., Fuel Cell Technology Handbook, Boca Raton, Fla.: CRC Press, c2003.

Kinoshita, K. and Stonehart, P., *Modern Aspects of Electrochemistry*, Vol.12, Bockris , J.O'M. and Conway, B.E., Eds., Plenum Press, New York, 1977, p. 183.

Klug, H. and Alexander, L., *X-ray Diffraction Procedures*, Wiley, New York, 1962.

Liebhavskky, H.A. and Cairns, E.J., *Fuel Cells and Fuel Batteries*, Wiley, New York, 1968.

Liu, Z., Ling, X.Y., Su, X., and Lee, J.Y., *Journal of Physical Chemistry B*, 108, 8234, 2004.

Linden, D., *Handbook of Fuel Cells and Fuel Batteries, ed. D. Linden*, McGraw Hill, New York, 1984.

McNicol, B. D., *Catalysis*, 2, 243, 1978.

McNicol, B.D., *Journal of Electroanalytical Chemistry*, 118, 71, 1981.

Mond, L. and Langer, C., *Proceedings of the Royal Society of London*, 46, 296, 1889.

Müller, E., *Z.Electrochem.,* 29, 264, 1923.

Müller, E. and Takegami, S., *Z.Electrochem.,* 34, 704, 1928.

Nefedov, V.I., *X-Ray Photoelectron Spectroscopy of Solid Surfaces, formly VNU Science Press BV*, The Netherlands, 1988

Nernst, W. *German Patents*, 259, 241, 1912.

Ostwald, W., *Zeitschrift für Elektrotechnik und Electrochemie*, 1, 122, 1894.

Peuckert, M., *Electrochimica Acta*, 29, 1315, 1984.

Peuckert, M., Coenem, F. P. and Bonzel, H. P., *Electrochimica Acta*, 1305, 1984.

Sen, F. and Gokagac, G., *J. Phys. Chem. C* , *111,* 1467, 2007.

Siegl, K., *Electrotech. Z.*, 34, 1317, 1913.

Tu, W., Takai, K., Fukui, K., Miyazaki, A. and Enoki, T., *J. Phys. Chem. B*, *107,* 10134, 2003.

Watanabe, M., Uchida, M., and Motoo, S., *Journal of Electroanalytical Chemistry*, 229, 395, 1987.

Weeks, S.A., *Doctor of Philosophy Thesis, University of Oxford, U.K.*, 1988.

Williams, D.B.and Carter, B.C., *Transmission Electron Microscopy a textbook for a material science*, Kluwer Academics, 1996.

Yee, C., Scotti, M., Ulman, A., White, H., Rafailovich M., and Sokolov, J., *Langmuir*, 15, 4314, 1999.

Zubraegel, C; Deuper, C.; Scheider, F.; Neumann, M.; Grunze, M.; Schertel, A. and Woll, C., *Chem. Phys. Lett*., 238, 308, 1995.